J Stat Phys (2007) 129: 335–376
DOI 10.1007/s10955-007-9359-0

A Statistical Mechanical Study of Current Spikes Due to Phase Transitions at Electrode-Electrolyte Interfaces

Igor Medved' · Dale A. Huckaby

Received: 9 November 2005 / Accepted: 17 November 2006 / Published online: 24 July 2007

Abstract We develop a statistical mechanical description of current spikes experimentally measured during first-order phase transitions on electrode surfaces. We interpret an experimental current spike as an averaged result of the finite-size effects for a large ensemble of crystalline domains (crystals) that are formed on the electrode surface, i.e., as an envelope of mutually shifted single-crystal spikes of various heights and widths. Rather than starting with a particular lattice gas model, we use rigorous results of Borgs and Kotecký on the finite-size effects valid for a large class of models to describe, in a unifying way, a spike corresponding to a first-order phase transition in a single crystal. We apply our results to fit theoretical spikes to experiment with very good precision. Whenever a phase transition is microscopically simulated by a lattice gas model, the data taken from experiment can be used to determine the strength of interactions in the model. As an illustration, we consider two experimental processes, both of which we model with the standard one-component lattice gas.

Keywords Voltammogram · First-order phase transition · Lattice gas

1 Introduction

1.1 The Current Spikes to be Studied

Measurements of electrochemical quantities such as a potential, current, charge, resistance, or capacitance use the fact that the measured quantity depends on the quality or the amount of the substance analyzed in a given electrochemical reaction. Voltammetry is an important electroanalytical method in which the reaction affects only a thin layer of the examined

I. Medved'
Department of Physics, Constantine the Philosopher University, 949 74 Nitra, Slovakia

D.A. Huckaby (✉)
Department of Chemistry, Texas Christian University, Fort Worth, TX 76129, USA
e-mail: d.huckaby@tcu.edu

solution in a small neighborhood of the indication electrode. The electrode is polarized by a controlled external electric potential ψ that varies linearly with time, $\psi = \psi_i + \nu t$, from an initial value ψ_i up to a final value $\psi_f > \psi_i$; the polarization speed

$$\nu \equiv \frac{d\psi}{dt} \tag{1.1}$$

is called the *scan rate*. In cyclic voltammetry the electrode polarization speed is reversed at ψ_f and the potential is linearly returned to its initial value ψ_i.

As ψ varies, a current flows through the electrode surface and the corresponding current density J is the measured electrochemical quantity. A *voltammogram* is a plot of the function $J(\psi)$. There are two main contributions to the current: (a) the Faradaic current—due to electrochemical reactions in the cell and the corresponding charge transfer occurring at the electrode surfaces; and (b) the capacitive current—due to (dis)charge of the electrical double layer capacitance of the electrode. The latter current does not involve any chemical reactions, it only causes accumulation (removal) of charge on and in the very vicinity of the electrode.

Bulk electrodeposition of a metal ion M^{+z} onto an electrode surface consisting of atoms of the *same* metal M begins at the equilibrium (Nernst) potential. When the potential ψ is increased above the Nernst value, bulk deposition does not occur. However, for some metals M it is possible to deposit the ion M^{+z} on an electrode of a *different*, more noble metal $M' \neq M$; for example, copper can be so deposited on a silver, gold, or platinum electrode surface. This phenomenon is called *underpotential deposition*, and it results in a *monolayer* or submonolayer deposition (once the metal ion is deposited on the electrode surface, it cannot be further deposited on itself), and *ordered* two-dimensional phases commensurate with the geometrical alignment of the electrode surface atoms are often observed.

A sudden deposition of a metallic (sub)monolayer on a crystalline electrode is represented by the presence of one or more sharp spikes in the associated voltammogram and can be interpreted as a phase transition at the electrode surface [1]. In this paper we present a statistical mechanical theory from which voltammogram spikes corresponding to first-order phase transitions can be obtained. Moreover, we apply our theory to experiment and show that macroscopic properties of a voltammogram spike determine the strength of microscopic interactions in a lattice gas that one may use to model the associated deposition process.

1.2 A Brief History of Results

Pioneering statistical mechanical studies of first-order phase transitions on electrode surfaces with a view to underpotential deposition are due to Blum and Huckaby. They introduced a lattice gas model [2] that successfully described the structure of phases experimentally observed in the underpotential deposition of Cu on Au(111) [2–5].[1] Nevertheless, their theoretical description of voltammogram spikes was not completely satisfactory because, using an *infinite* lattice of adsorption sites, they obtained infinitely tall and infinitely sharp spikes. They resolved the problem by adding a qualitative "switching function" [2, 6].

Underpotential deposition experiments have also been extensively modeled with the help of computer Monte Carlo simulations on lattice gases. The key works are due to Rikvold and coworkers (Refs. [7, 8] and papers referenced there), especially their study of the underpotential deposition of Cu on Au(111) in which two voltammogram spikes occur as the result

[1] The triplet 111 stands for the crystallographic Miller indices hkl.

of first-order phase transitions [9, 10]. Using a *finite* lattice of adsorption sites, they obtained voltammogram spikes of finite height and non-zero width that were in qualitative agreement with experiment, but the simulated spikes were still too tall and sharp at the transitions [9].

In our earlier works [11, 12] we carried out a statistical mechanical analysis of voltammogram spikes occurring during the underpotential deposition of Cu on Pt(111) and on Au(111), and we obtained results that were in very good qualitative and quantitative agreement with experiments. Our analysis was based on the observation that an electrode surface consisted of a large number of finite "crystalline domains" that we called *crystals*. It soon turned out that a voltammogram spike could not be a result of a first-order phase transition in a *single* crystal: the current density from a crystal exhibited a spike that was, for a "typical" crystal (several hundred sites in size), about a hundred times taller and sharper than the experimental one. However, due to finite-size effects spikes from various crystals are mutually shifted and of varying heights and widths, and the resulting average envelope of spikes can very well fit the profile of a voltammogram spike. Thus, we conjectured that it is this average that is actually measured and plotted in experiments, which led us to the following hypothesis:

(H) Each and every crystal contributes to the overall current density depending on the size of the crystal, its shape, and boundary conditions. A voltammogram spike is an *averaged result* of contributions coming from all the crystals.

Using the rigorous theory of Borgs and Kotecký [13] to control the finite-size behavior of the current density from a single crystal, the point then was to find a simple but physically plausible way in which the contributions from various crystals were to be put together so that theoretical and experimental voltammogram spikes agreed. From this viewpoint, a voltammogram spike may be simply interpreted as an averaged result of finite-size effects in an *ensemble* of crystals.

1.3 The Scope and Goals of the Present Paper

In this paper we continue in our statistical mechanical study of voltammogram spikes based on the hypothesis (H) with the aim to generalize our previous particular results and to make them readily applicable to a broader range of experiments.

We consider an electrode surface with a flow of current in it. We assume that the Faradaic part of the current is exclusively due to the discharge of a single type of ion and that any capacitive contributions can be neglected. Then the current density at the electrode interface is given as [3]

$$J(\psi) = -\kappa e_0 \gamma \nu \frac{\partial \Theta(\psi)}{\partial \psi}. \tag{1.2}$$

Here κ is the number of adsorption sites on the electrode surface per unit area, e_0 is the elementary charge, and ν is the scan rate. In addition, γ and Θ are the effective electrovalence and the coverage of the ion deposited on the electrode surface, respectively. The quantity γ relates the applied electric potential ψ to the chemical potential of the ion (c.f. (2.7)) and is considered independent of ψ. The coverage Θ is defined as the statistical average value of the fraction of adsorption sites occupied by the ion.

When the potential ψ is linearly increased from ψ_i to ψ_f, the ion is being stripped off of the electrode surface and the coverage $\Theta(\psi)$ decreases. Upon the reversal of ψ and its linear return to ψ_i, the ion is being deposited on the electrode surface and the coverage $\Theta(\psi)$ increases. The minus sign in (1.2) is thus chosen to ensure that the current density $J(\psi)$ is positive for the stripping process.

We will solely focus only on the stripping part of the deposition process, $\nu > 0$. This is due to the fact that our statistical mechanical analysis is, strictly speaking, valid only in equilibrium, i.e., in the "quasistatic" limit $\nu \to 0$, while at higher scan rates kinetic effects must be taken into account. Nevertheless, these effects should be rather less important in stripping processes that in the deposition ones.

In order to model a voltammogram spike, we assume that the current density $J(\psi)$ exhibits, as ψ varies, a spike that corresponds to a first-order transition between *two* phases to be denoted "+" and "−" in the sequel. However, unlike in Refs. [11] and [12], we do not start our analysis by considering a specific lattice gas model to describe first-order phase transitions in a specific experimental situation. Instead, we will use the rigorous Borgs–Kotecký theory [13] of finite-size effects near first-order phase transitions to show that, for a wide class of lattice models, namely, those that can be treated by the Pirogov–Sinai theory [14, 15], the behavior of the current density $j_C(\psi)$ from a single crystal C is remarkably universal. In particular, there are only three "mesoscopic" quantities (the crystal size S_C, a shape factor ξ_C, and a boundary tension τ_C, roughly speaking) that in essence fully characterize the current density $j_C(\psi)$ and whose values can vary from crystal to crystal. Combined with the hypothesis (H), the overall current density $J(\psi)$ becomes a *triple average* of the current densities $j_C(\psi)$ from all the crystals.

To evaluate this average, we suppose that the crystals do not mutually interact (since they are well separated by defects formed on the electrode surface) and that the number of adsorption sites that lie in the defect regions can be neglected with respect to their total number on the electrode surface. However, since the mechanisms determining the distributions of the values of the three quantities S_C, ξ_C, and τ_C largely depend on the experimental methods of preparation of the electrode surface, it may be hard to adopt sufficiently plain, yet physically plausible assumptions on the general behavior of these distributions. While we are basically able to do so in the case of τ_C, we will consider the value of ξ_C fixed (i.e., the crystals are considered of a uniform shape), making thus the corresponding average trivial, and leave the final average over the crystal sizes S_C unevaluated. Nevertheless, we provide two simple examples of the size distribution for which the size average can be easily evaluated. Moreover, in an appendix we argue that assuming the value of ξ_C constant can be checked from experimental data and is usually appropriate.

When wishing to apply our theory and fit an experimental voltammogram spike, it is useful to have a few macroscopic characteristics of the spike that can be easily measured as well as obtained from the theory. We consider these four characteristics:

- the spike's area $A \equiv \int_{-\infty}^{\infty} J(\psi)d\psi$,
- its maximum position $\psi_{\max}$,
- the height $H \equiv J(\psi_{\max})$, and
- an asymmetry factor $\alpha \equiv \frac{1}{A}\int_{-\infty}^{\psi_{\max}} J(\psi)d\psi \in (0, 1)$ (the relative area of $J(\psi)$ below $\psi_{\max}$).

We will derive approximative formulas from which these characteristics can be evaluated and describe a general strategy in which the theoretical current density can be fitted to an experimental voltammogram spike. The strategy is illustrated with three examples for which we also introduce a lattice gas model to microscopically simulate the phase transition. The strengths of interactions in the model are then calculated, using the experimental fitting data.

1.4 The Structure of the Paper

We start by giving a formal setting of the considered experimental situation in Sect. 2. Our main theoretical results are given in Sect. 3, including the evaluation of the triple average

in Statement 3.14. In Sect. 4 we show how our theory can be applied to experiment, using Statement 4.1. As an illustration, we fit, with very good agreement, the voltammogram spikes for the underpotential deposition of Cu on Pt(111) and on Pt(100). We also consider a lattice gas model simulating the two deposition processes and calculate the strengths of the involved microscopic interactions. A discussion of whether a voltammogram spike can in principle correspond to the current density from a single crystal and comments on the comparison of our theory with the intensive computer simulation studies of underpotential deposition by Rikvold and co-authors Refs. [7–10] are included. The verification of Statements 3.14 and 4.1 is deferred to Sect. 5 and Sect. 6, respectively. Finally, in Appendix we discuss the situation when the crystal shapes are not assumed uniform but can vary.

2 The Formal Setting

Let us first formally describe the experimental situation that was outlined in the Introduction and that we will analyze theoretically in the subsequent sections.

We assume that the array of adsorption sites on the electrode surface creates a regular two-dimensional lattice $\mathcal{L}$, such as a square or a triangular lattice. We will use $n_{\mathcal{L}}$ to denote the number of all nearest neighbors of a fixed site on the lattice $\mathcal{L}$; for instance, $n_{\mathbb{Z}^2} = 4$ for the square lattice $\mathcal{L} = \mathbb{Z}^2$.

Definition 2.1 A *crystal* C is a finite, simply connected subset of the lattice $\mathcal{L}$. We will use S_C to denote the number of sites in C and $\mathcal{C}_{\mathcal{L}}$ to denote the set of all crystals on $\mathcal{L}$.

2.1 The Class of the Considered Lattice Models

As was shown by Blum and Huckaby [2–6], the underpotential deposition of an ion on the electrode surface can be microscopically simulated by the behavior of a suitable lattice gas model.[2] Let $H_C^{\boldsymbol{\omega}}(\boldsymbol{\sigma})$ be the Hamiltonian of a lattice model for a configuration $\boldsymbol{\sigma}$ in the crystal C with boundary conditions $\boldsymbol{\omega}$. We will not introduce any particular Hamiltonian until Sect. 4.2, though. Instead, we will proceed in a more general fashion and work with a whole class of lattice models, namely, all the models that can be treated by the Pirogov–Sinai theory [14, 15].

The class is introduced by giving the form (given in Definition 2.4 below) into which it is possible to rewrite the grand-canonical partition function

$$Z_C^{\boldsymbol{\omega}}(\mu) \equiv \sum_{\boldsymbol{\sigma}} e^{-\beta[H_C^{\boldsymbol{\omega}}(\boldsymbol{\sigma}) - \mu S_C \mathrm{fr}(\boldsymbol{\sigma})]}, \quad \beta \equiv \frac{1}{k_B T}, \tag{2.1}$$

of each model in the class; here μ is the chemical potential for the adsorption of the ion on the electrode, $\mathrm{fr}(\boldsymbol{\sigma})$ is the number of sites in C occupied by the ion in the configuration $\boldsymbol{\sigma}$ divided by S_C, and β is the inverse temperature (T is the temperature and k_B is the Boltzmann constant). Thus, any lattice system whose partition function $Z_C^{\boldsymbol{\omega}}$ can be put into this form falls within the class. Let us now introduce the class precisely.

[2] For a thorough exposition on lattice systems, see [16], for example.

Definition 2.2 Let Γ_∞ be a countable set and let $\mathbb{I} \subset \Gamma_\infty \times \Gamma_\infty$ be a symmetric and reflexive relation. A set $\Gamma \subset \Gamma_\infty$ is compatible if $(\gamma_1, \gamma_2) \notin \mathbb{I}$ for any pair of distinct elements $\gamma_1, \gamma_2 \in \Gamma$.[3] Given $\Gamma \subset \Gamma_\infty$, we write $\mathrm{com}\,\Gamma$ for the set of all compatible subsets of Γ.

For any function $w : \Gamma_\infty \to \mathbb{C}$ and any finite set $\Gamma \subset \Gamma_\infty$ we define

$$\Xi(\Gamma, w) \equiv \sum_{\Gamma' \in \mathrm{com}\,\Gamma} \prod_{\gamma \in \Gamma'} w(\gamma), \tag{2.2}$$

where the summand corresponding to $\Gamma' = \emptyset$ is set equal to 1.

Remark 2.3 (i) The elements of the set Γ_∞ are usually called contours (or polymers), w is their weight, and Ξ is the corresponding contour (or polymer) partition function. Although there are rather canonic prescriptions [13–15], the set of contours Γ_∞, the relation $\mathbb{I}$, and the contour weight w are in principle introduced on a case-by-case basis, their definition being tailored to the particular situation.

(ii) Due to the very abstract and general definition, contour models are often met in the study of lattice models (see Remark 2.5(iv) below). There exist several, more or less equivalent methods to control perturbatively the logarithm of Ξ via a series called a cluster expansion [17–20]. The convergence of the series is guaranteed on condition that, for example, [17]

$$\sum_{\gamma' \in \Gamma_\infty : (\gamma', \gamma) \in \mathbb{I}} e^{(\bar{a}+\bar{d})(\gamma')} |w(\gamma')| \leqslant \bar{a}(\gamma) \quad \forall \gamma \in \Gamma_\infty \tag{2.3}$$

holds for some functions $\bar{a}, \bar{d} : \Gamma_\infty \to [0, \infty)$.

(iii) The condition (2.3) is usually true at sufficiently low temperatures (β large). This is the case when contours are introduced as finite connected subsets of $\mathcal{L}$ representing energetic barriers between ground states, the relation $\mathbb{I}$ means mutual intersection of contours, and $|w(\gamma)|$ behaves as $e^{-\mathrm{const}\,\beta|\gamma|}$, where $|\gamma|$ is the number of sites in the contour γ.[4] On the other hand, (2.3) does not always mean that β must be large enough. For example, for the q-state Potts model it means that $\log q$ must be large enough.

Definition 2.4 Let the following be given:

(a) a countable set Γ_∞ of contours (along with a symmetric and reflexive relation $\mathbb{I}$);
(b) a mapping Λ assigning a finite set $\Lambda(C) \subset \Gamma_\infty$ of contours to any crystal $C \in \mathcal{C}_\mathcal{L}$; and
(c) functions

$$\begin{aligned} &e_q : \mathcal{I} \to \mathbb{R}, \\ &e_q^{\boldsymbol{\omega}} : \{1, \dots, n_\mathcal{L} - 1\} \times \mathcal{I} \to \mathbb{R}, \quad \forall q \in Q \\ &w_q^{\boldsymbol{\omega}} : \Gamma_\infty \times \mathcal{I} \to \mathbb{R}, \end{aligned} \tag{2.4}$$

where Q is a finite set and $\mathcal{I} \subset \mathbb{R}$ is an open interval.

An abstract Pirogov–Sinai partition function in a crystal C is defined as

$$\mathcal{Z}_C^{\boldsymbol{\omega}}(\mu) \equiv \sum_{q \in Q} e^{-\beta E_q^{\boldsymbol{\omega}}(C, \mu)} \Xi(\Lambda(C), w_q^{\boldsymbol{\omega}}(\cdot, \mu)) \tag{2.5}$$

[3] An empty set or a set with a single element is also considered compatible.

[4] One may then take $\bar{a}(\gamma) = |\gamma|$ and $\bar{d}(\gamma) = \frac{1}{2}\,\mathrm{const}\,\beta|\gamma|$, for instance.

with

$$E_q^{\boldsymbol{\omega}}(C,\mu) \equiv e_q(\mu)S_C + \sum_{m=1}^{n_{\mathcal{L}}-1} e_q^{\boldsymbol{\omega}}(m,\mu)B_C^{(m)}. \tag{2.6}$$

Here $B_C^{(m)}$ is the number of those sites in C each of which has exactly $1 \leqslant m \leqslant n_{\mathcal{L}} - 1$ nearest neighbors lying in C, respectively.

We consider the class of all lattice models whose partition function $Z_C^{\boldsymbol{\omega}}(\mu)$ can be rewritten as an abstract Pirogov–Sinai partition function $\mathcal{Z}_C^{\boldsymbol{\omega}}(\mu)$ for some set Γ_∞, some mapping Λ, and some functions $e_q(\mu)$, $e_q^{\boldsymbol{\omega}}(m,\mu)$, and $w_q^{\boldsymbol{\omega}}(\gamma,\mu)$, where q attains only *two* values, $Q = \{+,-\}$.

Remark 2.5 (i) The set $\Lambda(C)$ is the set of contours in the crystal C. The function $e_q(\mu)$ is to be identified with the specific energy of the q-th ground state and $e_q^{\boldsymbol{\omega}}(m,\mu)$ with the boundary energy density in the q-th ground state associated with every site that has exactly $1 \leqslant m \leqslant n_{\mathcal{L}} - 1$ nearest neighbors lying in C. Then $E_q^{\boldsymbol{\omega}}(C,\mu)$ becomes the energy of the q-th ground state $\boldsymbol{\sigma}_q$ in the crystal C, i.e., $E_q^{\boldsymbol{\omega}}(C,\mu) = H_C^{\boldsymbol{\omega}}(\boldsymbol{\sigma}_q) - \mu S_C \mathrm{fr}(\boldsymbol{\sigma}_q)$, and (2.6) represents its bulk-boundary expansion.

(ii) The requirement that the energy density $e_q^{\boldsymbol{\omega}}(m,\mu)$ is in our setting uniquely determined by m restricts possible interaction potentials of the considered lattice models as well as possible boundary conditions $\boldsymbol{\omega}$. It is satisfied for potentials and boundary conditions that are translation invariant. A generalization to periodic potentials and boundary conditions is possible, but we shall not pursue this more complicated situation here.

(iii) Although the Borgs–Kotecký theory [13] is applicable also to situations with a multiple-phase coexistence, $|Q| > 2$, in this paper we focus on the simple case involving only two phases, $|Q| = 2$. Even for systems with $|Q| > 2$ it may be still true that only two of all the $|Q|$ phases are stable in the explored portion of the phase diagram (one is far away from triple points, for instance); we encountered such a situation in Ref. [12]. Then of all the summands in (2.5) only the two associated with the stable phases are dominant, and one effectively deals again with the situation $|Q| = 2$.

(iv) It turns out that the class of the Pirogov–Sinai models is quite rich. In particular, it contains all the lattice models with a translation invariant finite-range m-potential and a finite number of ground states. For a detailed exposition on the Pirogov–Sinai theory we refer the reader to the original works [13–15, 21] or to an overview article [22].

2.2 The Current Density from a Single Crystal

The single-crystal current density must be introduced in agreement with the expression (1.2) for the overall electrode current density $J(\psi)$. To this end, one needs to realize that, as the applied electric potential ψ varies, the chemical potential changes, $\mu = \mu(\psi)$. This dependence may be assumed to be linear [4],

$$\mu(\psi) = \mu_l(\psi) \equiv -e_0\gamma(\psi - \psi_0), \tag{2.7}$$

where the constants γ and ψ_0 are called the effective electrovalence of the ion deposited on the electrode surface and a reference potential, respectively. For simplicity, we will assume that (2.7) is valid for any $\psi \in \mathbb{R}$.

Definition 2.6 The coverage in a crystal C is the statistical average value of the fraction $\mathrm{fr}(\boldsymbol{\sigma})$ of occupied adsorption sites in C,

$$\theta_C^{\boldsymbol{\omega}}(\mu) \equiv \frac{1}{\mathcal{Z}_C^{\boldsymbol{\omega}}(\mu)} \sum_{\boldsymbol{\sigma}} \mathrm{fr}(\boldsymbol{\sigma}) e^{-\beta[H_C^{\boldsymbol{\omega}}(\boldsymbol{\sigma}) - \mu S_C \mathrm{fr}(\boldsymbol{\sigma})]}. \tag{2.8}$$

The current density from a crystal C is

$$j_C^{\boldsymbol{\omega}}(\psi) \equiv -\kappa e_0 \gamma \nu \frac{\partial \theta_C^{\boldsymbol{\omega}}(\mu_l(\psi))}{\partial \psi}, \tag{2.9}$$

where the constants κ, e_0, γ, and ν were introduced in (1.2).

From the definitions (2.8) and (2.9) it easily follows that

$$\begin{aligned} \theta_C^{\boldsymbol{\omega}}(\mu) &= \frac{1}{\beta S_C} \frac{\partial}{\partial \mu} \log \mathcal{Z}_C^{\boldsymbol{\omega}}(\mu), \\ j_C^{\boldsymbol{\omega}}(\psi) &= \frac{\kappa (e_0 \gamma)^2 \nu}{\beta S_C} \left[\frac{\partial^2}{\partial \mu^2} \log \mathcal{Z}_C^{\boldsymbol{\omega}}(\mu) \right]_{\mu = \mu_l(\psi)}. \end{aligned} \tag{2.10}$$

Here we also used that the partition function $Z_C^{\boldsymbol{\omega}}$ can be identified with a Pirogov–Sinai partition function $\mathcal{Z}_C^{\boldsymbol{\omega}}$.

2.3 Perturbative Control and the Existence of a Phase Transition

We want to apply the Borgs–Kotecký theory [13] in order to have a rigorous perturbative control over the partition function $\mathcal{Z}_C^{\boldsymbol{\omega}}(\mu)$ and thus, by virtue of (2.10), also over the coverage $\theta_C^{\boldsymbol{\omega}}(\mu)$ and the current density $j_C^{\boldsymbol{\omega}}(\psi)$ from a single crystal. In addition, to comply with the physical setting outlined in the Introduction, we need that $j_C^{\boldsymbol{\omega}}(\psi)$ exhibits a spike corresponding to a first-order phase transition. With these two ends in view, we adopt the following assumptions.

(As1) The functions $e_\pm(\mu)$ and $e_\pm^{\boldsymbol{\omega}}(m, \mu)$, $m = 1, \ldots, n_{\mathcal{L}} - 1$, are $C^4(\mathbb{R})$ functions of μ and their derivatives are uniformly bounded on $\mathbb{R}$,

$$\left| \frac{\partial^j e_\pm(\mu)}{\partial \mu^j} \right| \leqslant K_0^j, \qquad \left| \frac{\partial^j e_\pm^{\boldsymbol{\omega}}(m, \mu)}{\partial \mu^j} \right| \leqslant K_0^j, \quad \forall j = 1, \ldots, 4, \tag{2.11}$$

where the constant $K_0 > 0$ is independent of μ.[5] Moreover, the bound

$$\sup_{\mu \in \mathbb{R}} |e_+^{\boldsymbol{\omega}}(m, \mu) - e_-^{\boldsymbol{\omega}}(m, \mu)| \leqslant \lambda \frac{\bar{d}_0}{\beta} \tag{2.12}$$

is true for some $\lambda > 0$. Here

$$\bar{d}_0 \equiv \inf_{\gamma \in \Gamma_\infty} \bar{d}(\gamma), \tag{2.13}$$

where the function $\bar{d}(\gamma)$ was introduced in Remark 2.3(ii).

[5] The reason to require differentiability exactly up to the 4-th order is that we need the current density $j_C^{\boldsymbol{\omega}}(\psi)$ to be twice differentiable to locate its maximal value and that $j_C^{\boldsymbol{\omega}}(\psi)$ is already a second derivative of a thermodynamic potential (see (2.10)).

(As2) The weights $w^{\omega}_{\pm}(\gamma, \mu)$ are $C^4(\mathbb{R})$ functions of μ and the condition (2.3) holds.[6]

(As3) The bound

$$\xi_C \equiv \frac{B_C}{\sqrt{S_C}} \leqslant \hat{\xi}, \quad B_C \equiv \sum_{m=1}^{n_{\mathcal{L}}-1} B_C^{(m)}, \tag{2.14}$$

is satisfied for a (sufficiently small) constant $\hat{\xi} > 0$. Here B_C is the number of sites in the crystal C lying on its 1-boundary (having at least one nearest neighbor in $\mathcal{L}\backslash C$).

(As4) There exists a single value $\mu_0 \in \mathbb{R}$ of the chemical potential such that

$$e_+(\mu_0) = e_-(\mu_0). \tag{2.15}$$

Furthermore,

$$0 < K_1 \leqslant -\frac{\partial(e_+ - e_-)(\mu)}{\partial \mu} \leqslant K_2 \tag{2.16}$$

for all $\mu \in \mathbb{R}$ and some μ-independent constants $K_1 < K_2 < \infty$.

Remark 2.7 (i) The condition (2.12) permits only the "weak" boundary conditions $\boldsymbol{\omega}$ that would not strongly favor one of the two phases. The leading contributions to the partition function thus cannot contain large droplets — configurations in one phase in the bulk of a crystal and in the other phase near the crystal boundary.

(ii) If the condition (2.3) means that the temperature is sufficiently low (see Remark 2.3(iii)), then $\bar{d}_0 \propto \beta \gg 1$.

(iii) The dimensionless ratio ξ_C takes into account the shape of crystals. It attains, for a given lattice $\mathcal{L}$, a minimum $\check{\xi}$ (exceeding the value $2\sqrt{\pi}$ corresponding to the disk) and it increases as the crystal becomes more and more oblong. Hence, the bound (2.14) excludes crystals with too oblong shapes, and only crystals with parallelogram-like shapes are allowed. It is understood that $\hat{\xi} > \check{\xi}$.

The assumptions (As1–As3) ensure a perturbative control over $\mathcal{Z}^{\omega}_C(\mu)$. Namely, one can find a constant $b > 0$ and construct functions $f_{\pm}(\mu)$ and $f^{\omega}_{\pm}(m, \mu)$, $m = 1, \ldots, n_{\mathcal{L}} - 1$, that are $C^4(\mathbb{R})$ functions of μ such that[7] [13]

$$\begin{aligned} \frac{\partial^j f_{\pm}(\mu)}{\partial \mu^j} &= \frac{\partial^j e_{\pm}(\mu)}{\partial \mu^j} + O(e^{-b\bar{d}_0}), \\ \frac{\partial^j f^{\omega}_{\pm}(m, \mu)}{\partial \mu^j} &= \frac{\partial^j e^{\omega}_{\pm}(m, \mu)}{\partial \mu^j} + O(e^{-b\bar{d}_0}), \quad \forall j = 0, \ldots, 4. \end{aligned} \tag{2.17}$$

[6] In fact, a generalization of (2.3) to the derivatives of the weights with respect to μ is also necessary. Instead of its precise formulation, we refer the reader to Ref. [13] (see also Remark (iii) in the Appendix of Ref. [23] and Proposition A.1 in Ref. [24]).

[7] We use the symbol $O(y)$ to denote an error term that can be uniformly bounded by const y, where the constant does not depend on μ, β, or a crystal C.

In addition,

$$\frac{\partial^j \mathcal{Z}_C^{\omega}(\mu)}{\partial \mu^j} = \left[\frac{\partial^j}{\partial \mu^j}(e^{-\beta F_+^{\omega}(C,\mu)} + e^{-\beta F_-^{\omega}(C,\mu)})\right](1 + S_C^j O(e^{-b\tilde{d}_0\sqrt{S_C}}))$$
$$\forall j = 0, \ldots, 4 \tag{2.18}$$

for all $\mu \in \mathbb{R}$, where

$$F_{\pm}^{\omega}(C,\mu) \equiv f_{\pm}(\mu) S_C + \sum_{m=1}^{n_{\mathcal{L}}-1} f_{\pm}^{\omega}(m,\mu) B_C^{(m)}. \tag{2.19}$$

The bound (2.18) immediately implies that the free energy

$$f(\mu) \equiv -\frac{1}{\beta} \lim_{C \nearrow \mathcal{L}} \frac{1}{S_C} \log \mathcal{Z}_C^{\omega}(\mu) \tag{2.20}$$

exists (the limit $C \nearrow \mathcal{L}$ is in the van Hove sense due to (2.14)), and

$$f(\mu) = \min\{f_+(\mu), f_-(\mu)\}. \tag{2.21}$$

Remark 2.8 According to (2.18), the partition function in a crystal C in which the phases $+$ and $-$ coexist can be with a great precision expressed as

$$\mathcal{Z}_C^{\omega}(\mu) \approx e^{-\beta F_+^{\omega}(C,\mu)} + e^{-\beta F_-^{\omega}(C,\mu)}. \tag{2.22}$$

The "free energies" $F_{\pm}^{\omega}(C,\mu)$ of the $(\pm)$-phase deviate only slightly from the corresponding "ground-state energies" $E_{\pm}^{\omega}(C,\mu)$ defined in (2.6) in the sense that they possess the same kind of a bulk-boundary expansion (2.19), and the "specific free energies" $f_{\pm}(\mu)$ and the "boundary free energy densities" $f_{\pm}^{\omega}(m,\mu)$, including their derivatives, are in view of (2.17) very well approximated by the corresponding "specific energies" $e_{\pm}(\mu)$ and the "boundary energy densities" $e_{\pm}^{\omega}(m,\mu)$.

The assumption (As4) is added to ensure the presence of a first-order phase transition; this is a standard result of the Pirogov–Sinai theory [13–15]. Precisely, there exists a point $\mu_{\mathrm{tr}} \in \mathbb{R}$ (the infinite-volume transition point) such that the free energy $f(\mu)$ has a discontinuous derivative at μ_{tr}. The point μ_{tr} is very close to μ_0,

$$\mu_{\mathrm{tr}} = \mu_0 + O(e^{-b\tilde{d}_0}). \tag{2.23}$$

The unique point ψ_{tr} associated with μ_{tr} through the linear mapping $\mu_l(\psi)$ introduced in (2.7) is

$$\psi_{\mathrm{tr}} = \psi_0 - \frac{\mu_{\mathrm{tr}}}{e_0 \gamma}. \tag{2.24}$$

Remark 2.9 In fact, the point μ_{tr} is defined by the equality $f_+(\mu_{\mathrm{tr}}) = f_-(\mu_{\mathrm{tr}})$ (both phases are stable at μ_{tr}), and then (2.23) readily follows from (2.15) and (2.17). The discontinuity of the derivative of $f(\mu)$ at thus defined μ_{tr} is a consequence of (2.17), (2.21), and the degeneracy-removing condition (2.16). Indeed, $f(\mu)$ equals $f_+(\mu)$ above μ_{tr} and $f_-(\mu)$

below $\mu_{\rm tr}$ (the difference $(f_+ - f_-)(\mu)$ is decreasing, $-\frac{\partial(f_+-f_-)(\mu)}{\partial\mu} \geqslant K_1 + O(e^{-b\tilde{d}_0}) > 0$ on $\mathbb{R}$) so that

$$-\left[\frac{\partial f(\mu_{\rm tr}+0)}{\partial\mu} - \frac{\partial f(\mu_{\rm tr}-0)}{\partial\mu}\right] = -\frac{\partial(f_+ - f_-)(\mu_{\rm tr})}{\partial\mu} > 0. \tag{2.25}$$

This can be also expressed as a discontinuity in the infinite-volume coverage

$$\theta(\mu) \equiv \lim_{C\nearrow\mathcal{L}} \theta_C^{\boldsymbol{\omega}}(\mu), \tag{2.26}$$

namely,

$$\theta(\mu_{\rm tr}+0) - \theta(\mu_{\rm tr}-0) = -\frac{\partial(f_+ - f_-)(\mu_{\rm tr})}{\partial\mu} > 0. \tag{2.27}$$

The equalities

$$\frac{\partial^j\theta(\mu)}{\partial\mu^j} = -\frac{\partial^{j+1}f(\mu)}{\partial\mu^{j+1}} = \begin{cases} -\frac{\partial^{j+1}f_+(\mu)}{\partial\mu^{j+1}}, & \mu\in(\mu_{\rm tr},\infty), \\ -\frac{\partial^{j+1}f_-(\mu)}{\partial\mu^{j+1}}, & \mu\in(-\infty,\mu_{\rm tr}), \end{cases} \quad \forall j = 0,\dots,3 \tag{2.28}$$

are a consequence of (2.18). The fact the discontinuity (2.27) is positive (i.e., that the $+$ phase is stable above $\mu_{\rm tr}$, while the $-$ phase is stable below it, and not the opposite) is just a matter of choice made in (2.16).

2.4 Electrode Current Density $J(\psi)$ as an Average

We imagine that a large but finite ensemble $\mathcal{C}_E \subset \mathcal{C}_\mathcal{L}$ of crystals is given; the ensemble represents the collection of all crystals lying on the electrode surface. We also imagine that some fixed boundary conditions $\boldsymbol{\omega}_E$ for the union $E \equiv \cup_{C\in\mathcal{C}_E} C \subset \mathcal{L}$ is given; it represents the interaction of the crystals with the parts of the electrode surface that separate the crystals from each other (i.e., with the defect regions on the electrode surface).[8] The restriction $\boldsymbol{\omega}_E(C)$ of $\boldsymbol{\omega}_E$ to the outer neighborhood of a crystal C constitutes the boundary conditions for that crystal.

The crystals of the ensemble are assumed not to mutually interact so that the partition function for the whole ensemble becomes the product of the partition functions of individual crystals,

$$Z_E^{\boldsymbol{\omega}_E}(\mu) = \prod_{C\in\mathcal{C}_E} \mathcal{Z}_C^{\boldsymbol{\omega}_E(C)}(\mu). \tag{2.29}$$

The total electrode coverage

$$\Theta_E^{\boldsymbol{\omega}_E}(\mu) \equiv \frac{1}{Z_E^{\boldsymbol{\omega}_E}(\mu)} \sum_{\boldsymbol{\sigma}_E} \mathrm{fr}(\boldsymbol{\sigma}_E) e^{-\beta[H_E^{\boldsymbol{\omega}_E}(\boldsymbol{\sigma}_E) - \mu S_{\rm tot}\mathrm{fr}(\boldsymbol{\sigma}_E)]} = \frac{1}{\beta S_{\rm tot}} \frac{\partial}{\partial\mu} \log Z_E^{\boldsymbol{\omega}_E}(\mu), \tag{2.30}$$

where the sum runs over the configurations $\boldsymbol{\sigma}_E$ on E, and $\mathrm{fr}(\boldsymbol{\sigma}_E)$ is the number of sites from E that are occupied in $\boldsymbol{\sigma}_E$ divided by the total number $S_{\rm tot} \equiv \sum_{C\in\mathcal{C}_E} S_C$ of adsorption sites.

[8] As was pointed out in Refs. [11, 12], periodic boundary conditions are inappropriate to consider, for they lead to results in evident disagreement with experiments.

Combined with the definition (1.2) and (2.10), we obtain [12]

$$\Theta_E^{\boldsymbol{\omega}_E}(\mu) = \langle \theta_C^{\boldsymbol{\omega}_E(C)}(\mu) \rangle_{\mathcal{C}}, \qquad J_E^{\boldsymbol{\omega}_E}(\psi) = \langle j_C^{\boldsymbol{\omega}_E(C)}(\psi) \rangle_{\mathcal{C}} \tag{2.31}$$

with

$$\langle \cdot \rangle_{\mathcal{C}} \equiv \sum_{C \in \mathcal{C}_E} \cdot \mathbb{P}_C, \quad \mathbb{P}_C \equiv \frac{S_C}{S_{\text{tot}}}. \tag{2.32}$$

The electrode coverage $\Theta_E^{\boldsymbol{\omega}_E}$ and current density $J_E^{\boldsymbol{\omega}_E}$ thus become averages of the coverages $\theta_C^{\boldsymbol{\omega}_E(C)}$ and current densities $j_C^{\boldsymbol{\omega}_E(C)}$ from the crystals under the discrete probability distribution $\{\mathbb{P}_C\}$.

3 Results

In this section we formulate our main theoretical results. Their verification is also provided here, with the exception of Statement 3.14 that is verified in Sect. 5.

3.1 The Finite-Size Effects for a Single Crystal

We begin with the analysis of the coverage $\theta_C^{\boldsymbol{\omega}}(\mu)$ and the current density $j_C^{\boldsymbol{\omega}}(\psi)$ associated with a single crystal C.

Definition 3.1 Let us introduce the shorthands

$$\theta_\pm(\mu) \equiv -\frac{\partial f_\pm(\mu)}{\partial \mu}, \qquad \theta_\pm^{\text{tr}} \equiv \theta_\pm(\mu_{\text{tr}}), \tag{3.1}$$

$$h \equiv \frac{a^2}{4\kappa\nu}, \qquad a \equiv (\theta_+^{\text{tr}} - \theta_-^{\text{tr}})\kappa e_0 \gamma \nu. \tag{3.2}$$

Moreover, let

$$s_C^{\boldsymbol{\omega}} \equiv \sum_{m=1}^{n_{\mathcal{L}}-1} [f_+^{\boldsymbol{\omega}}(m, \mu_{\text{tr}}) - f_-^{\boldsymbol{\omega}}(m, \mu_{\text{tr}})] \frac{B_C^{(m)}}{B_C}. \tag{3.3}$$

Remark 3.2 (i) The quantity $\theta_\pm(\mu)$ represents the infinite-lattice coverage of the ion deposited on the electrode surface in the $(\pm)$-phase (c.f. (2.26)) and $\theta_\pm^{\text{tr}}$ is its value at the transition point μ_{tr}.

(ii) The quantity $s_C^{\boldsymbol{\omega}}$ represents the difference of boundary contributions to the free energies of the plus and the minus phases at μ_{tr}. The value of $s_C^{\boldsymbol{\omega}}$ is determined by the boundary conditions $\boldsymbol{\omega}$, i.e., by the details of the interactions of the crystal C with its surroundings. Recalling that $\boldsymbol{\omega}$ is in turn determined by the electrode defects, and these defects in general change across the electrode surface, the value of $s_C^{\boldsymbol{\omega}}$ varies from crystal to crystal. Notice that $s_C^{\boldsymbol{\omega}}$ behaves as a *constant* with respect to the size S_C of the crystal as $C \nearrow \mathcal{L}$.

Employing the rigorous theory of finite-size effects near first-order phase transitions developed by Borgs and Kotecký [13], based in our situation on the bounds (2.17) and (2.18) and the expressions (2.10), we obtain the following results.

Statement 3.3 *Let* (As1)–(As4) *be true and let* S_C *be sufficiently large.*

(1) *There exists a unique point,* $\psi_C^{\boldsymbol{\omega}}$*, at which* $j_C^{\boldsymbol{\omega}}(\psi)$ *attains its maximal value. Introducing* $\tau_C^{\boldsymbol{\omega}}$ *through the equality*

$$\psi_C^{\boldsymbol{\omega}} \equiv \psi_{\mathrm{tr}} - \frac{a\tau_C^{\boldsymbol{\omega}}}{4h}\frac{\xi_C}{\sqrt{S_C}}, \tag{3.4}$$

it follows that

$$\tau_C^{\boldsymbol{\omega}} = s_C^{\boldsymbol{\omega}}\left[1 + O\left(\frac{1}{\sqrt{S_C}}\right)\right]. \tag{3.5}$$

(2) *We have*

$$\theta_C^{\boldsymbol{\omega}}(\mu) = \frac{\theta_+(\mu)+\theta_-(\mu)}{2} + \frac{\theta_+(\mu)-\theta_-(\mu)}{2}\tanh\left[\frac{2h\beta S_C}{a}\frac{\mu-\mu_C^{\boldsymbol{\omega}}}{e_0\gamma}\right] + O\left(\frac{1}{\sqrt{S_C}}\right), \tag{3.6}$$

where $\mu_C^{\boldsymbol{\omega}} \equiv \mu_l(\psi_C^{\boldsymbol{\omega}})$ *is the chemical potential corresponding to* $\psi_C^{\boldsymbol{\omega}}$ *via* (2.7)*. Moreover,*

$$j_C^{\boldsymbol{\omega}}(\psi) = h\beta S_C \cosh^{-2}\left[\frac{2h\beta S_C}{a}(\psi - \psi_C^{\boldsymbol{\omega}})\right] + O(\sqrt{S_C}). \tag{3.7}$$

Remark 3.4 (i) The point $\psi_C^{\boldsymbol{\omega}}$ is shifted with respect to the infinite-lattice transition point ψ_{tr} by an amount proportional to $\frac{1}{\sqrt{S_C}}$. The shift is a pure finite-size effect, since the ratio $\frac{a}{h} = \frac{4}{(\theta_+^{\mathrm{tr}}-\theta_-^{\mathrm{tr}})e_0\gamma}$ is independent of the scan rate ν.

(ii) In view of (3.7), the single-crystal current density $j_C^{\boldsymbol{\omega}}(\psi)$ exhibits (very precisely) a *symmetric* spike around $\psi_C^{\boldsymbol{\omega}}$ within the region of width $O(\frac{1}{\beta S_C})$ that is much smaller than the shift $|\psi_C^{\boldsymbol{\omega}} - \psi_{\mathrm{tr}}|$. The spike is described by the function $\cosh^{-2}$. In view of (3.6), around the point $\mu_C^{\boldsymbol{\omega}}$ corresponding to $\psi_C^{\boldsymbol{\omega}}$ the coverage $\theta_C^{\boldsymbol{\omega}}(\mu)$ abruptly but smoothly interpolates between $\theta_+(\mu)$ and $\theta_-(\mu)$. The passage from one to the other takes place within the same region and is described by the function tanh.

(iii) Farther away from $\psi_C^{\boldsymbol{\omega}}$ (for $|\psi - \psi_C^{\boldsymbol{\omega}}| \geqslant O(\frac{1}{\sqrt{S_C}})$), when only one of the two phases is stable, the coverage $\theta_C^{\boldsymbol{\omega}}(\mu)$ and the current density $j_C^{\boldsymbol{\omega}}(\psi)$ are very well approximated by their infinite-volume limits $\theta(\mu)$ (see (2.26)) and $j(\psi) \equiv -\kappa e_0\gamma\nu\frac{\theta(\mu_l(\psi))}{\partial\psi}$, respectively. In both cases the error terms are of the order $O(\frac{1}{\sqrt{S_C}})$ [13].

(iv) The influence of the boundary conditions $\boldsymbol{\omega}$ on $j_C^{\boldsymbol{\omega}}(\psi)$ is basically limited to the position of the maximum $\psi_C^{\boldsymbol{\omega}}$. Hence, a different choice of $\boldsymbol{\omega}$ results in the possible shift of the function $j_C^{\boldsymbol{\omega}}(\psi)$, but its profile remains practically unchanged. The same is also true for $\theta_C^{\boldsymbol{\omega}}(\mu)$.

(v) In view of (3.3) and (3.5), the quantity $\tau_C^{\boldsymbol{\omega}}$ is associated with the boundary tension (the boundary free energy difference per unit length) in the crystal C that has the boundary conditions $\boldsymbol{\omega}$. It should be pointed out that $\tau_C^{\boldsymbol{\omega}}$ contains only a part of the information on the shape of a crystal C. In fact, the dominant factor should be the process of the experimental preparation of the electrode, upon completion of which the crystals are already formed on

the electrode surface, i.e., *before* the deposition of a metal ion on the surface is carried out. That is why we choose to consider the shape factor ξ_C as being independent of τ_C^{ω}.

(vi) From (3.6) it follows that the shorthand h has the meaning of the height of the spike exhibited by $j_C^{\omega}(\psi)$ for a crystal of unit size at $\beta = 1$, while a and is the area of this spike within the interval $|\psi - \psi_C^{\omega}| \geqslant O(\frac{1}{\sqrt{S_C}})$.

Besides the maximum point ψ_C^{ω}, further characteristics of the single-crystal current density $j_C^{\omega}(\psi)$ can be readily obtained from Statement 3.3.

Consequence 3.5 *Let* (As1)–(As4) *be true and let S_C be sufficiently large. The height and the half-width* (*the width at the half of the height*) *of the spike exhibited by $j_C^{\omega}(\psi)$ is*

$$\begin{aligned} H_C^{\omega} &\equiv j_C^{\omega}(\psi_C^{\omega}) = h\beta S_C\left[1 + O\left(\frac{1}{\sqrt{S_C}}\right)\right], \\ W_C^{\omega} &= \frac{\log(\sqrt{2}+1)a}{h\beta S_C}\left[1 + O\left(\frac{1}{\sqrt{S_C}}\right)\right]. \end{aligned} \tag{3.8}$$

The area under the spike is

$$A_C^{\omega} \equiv \int_{\mathbb{R}} j_C^{\omega}(\psi)d\psi = \kappa e_0 \gamma \nu[\theta(\infty) - \theta(-\infty)]\left[1 + O\left(\frac{1}{\sqrt{S_C}}\right)\right], \tag{3.9}$$

where $\theta(\mu)$ is the infinite-volume coverage (2.26).

Proof The bounds (3.8) follow directly from (3.7). In order to verify (3.9), it suffices to observe that, by (2.9),

$$\frac{A_C^{\omega}}{\kappa e_0 \gamma \nu} = -\int_{\mathbb{R}} \frac{\partial \theta_C^{\omega}(\mu_l(\psi))}{\partial \psi} d\psi = \int_{\mathbb{R}} \frac{\partial \theta_C^{\omega}(\mu)}{\partial \mu} d\mu = \theta_C^{\omega}(\infty) - \theta_C^{\omega}(-\infty) \tag{3.10}$$

and combine it with Remark 3.4(iii). □

3.2 The Finite-Size Effects for the Ensemble $\mathcal{C}_E$ of Crystals

Using the equalities (2.31) and Statement 3.3, we may obtain expressions for the electrode coverage $\Theta_E^{\omega_E}(\mu)$ and the electrode current density $J_E^{\omega_E}(\psi)$. However, the bounds (3.6) and (3.7) from Statement 3.3 that describe the behavior of single-crystal coverage $\theta_C^{\omega}(\mu)$ and current density $j_C^{\omega}(\psi)$ are valid only for crystals C with a sufficiently large number S_C of adsorption sites. Nevertheless, we will use these two bounds also for crystals of small sizes, assuming thus that this only insignificantly affects the values of the averages (2.31).

(As5) Let $\tilde{\theta}_C^{\omega}(\mu)$ and $\tilde{j}_C^{\omega}(\psi)$ be the functions on the right-hand side of (3.6) and (3.7), respectively. We assume that

$$\Theta_E^{\omega_E}(\mu) = \langle \tilde{\theta}_C^{\omega_E(C)}(\mu)\rangle_C, \qquad J_E^{\omega_E}(\psi) = \langle \tilde{j}_C^{\omega_E(C)}(\psi)\rangle_C, \tag{3.11}$$

where the average $\langle\cdot\rangle_C$ was defined in (2.32).

Remark 3.6 In Ref. [11] we showed numerically for an Ising system in a $n \times n$ parallelogram-shaped portion of a two-dimensional triangular lattice that the bounds (3.6) and (3.7) are good approximations of the true single-crystal coverage and current density for $n \gtrsim 4$.

Statement 3.7 *Assume* (As1)–(As5). *Then*

$$\Theta_E^{\omega_E}(\mu) = \frac{\theta_+(\mu)+\theta_-(\mu)}{2} + \frac{\theta_+(\mu)-\theta_-(\mu)}{2}\left\langle \tanh\left[\frac{2h\beta S_C}{a}\frac{\mu-\mu_C^{\omega}}{e_0\gamma}\right]\right\rangle_C + O\left(\left\langle\frac{1}{\sqrt{S_C}}\right\rangle_C\right), \tag{3.12}$$

and

$$J_E^{\omega_E}(\psi) = h\beta\left\langle S_C \cosh^{-2}\left[\frac{2h\beta S_C}{a}(\psi-\psi_C^{\omega})\right]\right\rangle_C + O(\langle\sqrt{S_C}\rangle_C). \tag{3.13}$$

Moreover, the area

$$A_E^{\omega_E} \equiv \int_{\mathbb{R}} J_E^{\omega_E}(\psi)d\psi = \kappa e_0\gamma\nu[\theta(\infty)-\theta(-\infty)]\left[1+O\left(\left\langle\frac{1}{\sqrt{S_C}}\right\rangle_C\right)\right]. \tag{3.14}$$

Proof It suffices to use the bounds (3.6), (3.7), and (3.9) and the identity $A_E^{\omega_E} = \langle A_C^{\omega_E(C)}\rangle_C$. □

Remark 3.8 Since the leading term $\kappa e_0\gamma\nu[\theta(\infty)-\theta(-\infty)]$ of the area of the spike exhibited by $j_C^{\omega}(\psi)$ is crystal-independent, it coincides with the leading term of the area under the total current density $J_E^{\omega_E}(\psi)$. In addition, the term is independent of the boundary conditions $\boldsymbol{\omega}_E$.

3.3 Evaluation of the Average $\langle\cdot\rangle_C$

Classifying the crystals according to their values of S_C, τ_C^{ω}, and ξ_C, the average $\langle\cdot\rangle_C$ may be alternatively expressed as a triple average. We will conveniently use this alternative expression to evaluate and analyze the properties of the coverage $\Theta_E^{\omega_E}(\mu)$ and the current density $J_E^{\omega_E}(\psi)$.

Definition 3.9 Let

$$\begin{aligned}\mathcal{S}_E &\equiv \{S\in\mathbb{N} : \exists C\in\mathcal{C}_E, S_C = S\},\\ \mathcal{T}_E &\equiv \{\tau\in\mathbb{R} : \exists C\in\mathcal{C}_E, \tau_C^{\omega_E(C)} = \tau\},\\ \mathcal{X}_E &\equiv \{\xi\in[\check{\xi},\hat{\xi}] : \exists C\in\mathcal{C}_E, \xi_C = \xi\}.\end{aligned} \tag{3.15}$$

For any $S\in\mathcal{S}_E$, $\tau\in\mathcal{T}_E$, and $\xi\in\mathcal{X}_E$ we introduce

$$\begin{aligned}\mathcal{C}_E^S &\equiv \{C\in\mathcal{C}_E : S_C = S\},\\ \mathcal{C}_E^{S,\tau} &\equiv \{C\in\mathcal{C}_E : S_C = S\wedge\tau_C^{\omega_E(C)} = \tau\},\\ \mathcal{C}_E^{S,\tau,\xi} &\equiv \{C\in\mathcal{C}_E : S_C = S\wedge\tau_C^{\omega_E(C)} = \tau\wedge\xi_C = \xi\}\end{aligned} \tag{3.16}$$

and the discrete probability distributions $\{\mathbb{P}_S\}$, $\{\mathbb{P}_\tau^{(S)}\}$, and $\{\mathbb{P}_\xi^{(S,\tau)}\}$ as

$$\mathbb{P}_S \equiv \frac{|\mathcal{C}_E^S|S}{S_{\mathrm{tot}}}, \qquad \mathbb{P}_\tau^{(S)} \equiv \frac{|\mathcal{C}_E^{S,\tau}|}{|\mathcal{C}_E^S|}, \qquad \mathbb{P}_\xi^{(S,\tau)} \equiv \frac{|\mathcal{C}_E^{S,\tau,\xi}|}{|\mathcal{C}_E^{S,\tau}|}, \tag{3.17}$$

respectively. Here $|\cdot|$ stands for the cardinality of the set.

Remark 3.10 Notice that $\mathbb{P}_S$ is the fraction of adsorption sites lying in crystals of the size $S_C = S$. Moreover, $\mathbb{P}_\tau^{(S)}$ is the fraction of crystals for which $S_C = S$ and the boundary tension $\tau_C^{\omega_E(C)} = \tau$. Finally, $\mathbb{P}_\xi^{(S,\tau)}$ is the fraction of crystals for which $S_C = S$, $\tau_C^{\omega_E(C)} = \tau$, and $\xi_C = \xi$.

Statement 3.11 *Let a function $f_C : \mathcal{S}_E \times \mathcal{T}_E \times \mathcal{X}_E \to \mathbb{R}$ be given. Then*

$$\langle f_C \rangle_C = \langle \langle \langle f_C(S, \tau, \xi) \rangle_\xi \rangle_\tau \rangle_S, \tag{3.18}$$

where

$$\langle \cdot \rangle_S \equiv \sum_{S \in \mathcal{S}_E} \cdot \mathbb{P}_S, \qquad \langle \cdot \rangle_\tau \equiv \sum_{\tau \in \mathcal{T}_E} \cdot \mathbb{P}_\tau^{(S)}, \qquad \langle \cdot \rangle_\xi \equiv \sum_{\xi \in \mathcal{X}_E} \cdot \mathbb{P}_\xi^{(S,\tau)} \tag{3.19}$$

are the averages under the probability distributions $\{\mathbb{P}_S\}$, $\{\mathbb{P}_\tau^{(S)}\}$, and $\{\mathbb{P}_\xi^{(S,\tau)}\}$, respectively.

Proof The statement easily follows from the definition (2.32) of the average $\langle \cdot \rangle_C$ and the obvious identity $\frac{S}{S_{\text{tot}}} |\mathcal{C}_E^{S,\tau,\xi}| = \mathbb{P}_S \mathbb{P}_\tau^{(S)} \mathbb{P}_\xi^{(S,\tau)}$. □

Remark 3.12 (i) In view of (3.4), the maximum position $\psi_C^{\boldsymbol{\omega}}$ of the single-crystal current density $j_C^{\boldsymbol{\omega}}(\psi)$ is a function on $\mathcal{S}_E \times \mathcal{T}_E \times \mathcal{X}_E$, namely,

$$\psi_C^{\boldsymbol{\omega}} = \psi_C(S_C, \tau_C^{\boldsymbol{\omega}}, \xi_C) \quad \text{with } \psi_C(S, \tau, \xi) \equiv \psi_{\text{tr}} - \frac{a\tau}{4h} \frac{\xi}{\sqrt{S}}. \tag{3.20}$$

Combined with (3.7), we get

$$j_C^{\boldsymbol{\omega}}(\psi) = j_C(S_C, \tau_C^{\boldsymbol{\omega}}, \xi_C, \psi) + O(\sqrt{S_C}), \tag{3.21}$$

where

$$j_C(S, \tau, \xi, \psi) \equiv h\beta S \cosh^{-2}\left[\frac{2h\beta S}{a} (\psi - \psi_C(S, \tau, \xi)) \right]. \tag{3.22}$$

A similar expression can also be obtained for the coverage $\theta_C^{\boldsymbol{\omega}}(\mu)$.

(ii) As soon as the distributions $\{\mathbb{P}_S\}$, $\{\mathbb{P}_\tau^{(S)}\}$, and $\{\mathbb{P}_\xi^{(S,\tau)}\}$ are known, $\Theta_E^{\boldsymbol{\omega}_E}$ and $J_E^{\boldsymbol{\omega}_E}$ can be evaluated (analytically or at least numerically) from (3.18). The latter equation shows that the electrode coverage $\Theta_E^{\boldsymbol{\omega}_E}$ and current density $J_E^{\boldsymbol{\omega}_E}$ may be interpreted as averages of "typical" coverages and current densities, respectively, from crystals of size S. The word typical means, however, that the averages over τ and ξ have already been taken.

(iii) In view of (3.18), the error terms $O(\langle \frac{1}{\sqrt{S_C}} \rangle_C)$ and $O(\langle \sqrt{S_C} \rangle_C)$ in (3.12) through (3.14) may be expressed as $O(\langle \frac{1}{\sqrt{S}} \rangle_S)$ and $O(\langle \sqrt{S} \rangle_S)$, respectively.

Present-day experiments do not provide much insight as to explicit forms of the distributions $\{\mathbb{P}_S\}$, $\{\mathbb{P}_\tau^{(S)}\}$, and $\{\mathbb{P}_\xi^{(S,\tau)}\}$. Therefore, in order to proceed, we shall consider the following simple, yet physically plausible scenario.

(As6) We neglect possible shape variations of crystals by assuming that ξ_C has a constant value, ξ_0, for all the crystals. Then (3.18) becomes

$$\langle f_C\rangle_C = \langle\langle f_C(S,\tau,\xi_0)\rangle_\tau\rangle_S. \tag{3.23}$$

(As7) For all $\mu\in\mathbb{R}$ we assume that

(a) the values from $\mathcal{T}_E$ are within an interval of length proportional to $S^{-1/4}$,

$$\begin{aligned}&\mathcal{T}_E\subset[\tau_0-w_\tau,\tau_0+w_\tau],\\ &\tau_0\in\mathbb{R},\quad \frac{\bar w_1}{S^{1/4}}\leqslant w_\tau\leqslant\frac{\bar w_2}{S^{1/4}}\quad(0<\bar w_1<\bar w_2<\infty);\end{aligned} \tag{3.24}$$

(b) the mesh size $\Delta\tau>0$, i.e., the maximal distance between two adjacent elements of $\mathcal{T}_E$, tends to zero,

$$\Delta\tau\to 0; \tag{3.25}$$

(c) for each $S\in\mathcal{S}_E$ there are piecewise differentiable functions $\mathcal{P}_S$, $p_S:\mathbb{R}\to[0,\infty)$ such that

$$\mathcal{P}_S(\tau)=\mathbb{P}_\tau^{(S)}\quad\forall\tau\in\mathcal{T}_E, \tag{3.26a}$$

$$\mathcal{P}_S(\tau)=0\quad\forall\tau\in\mathbb{R}\backslash[\tau_0-w_\tau,\tau_0+w_\tau], \tag{3.26b}$$

$$\lim_{\Delta\tau\to0}\frac{\mathcal{P}_S(\tau)}{\Delta\tau}=p_S(\tau),\qquad \frac{M_1}{w_\tau}\leqslant\sup_{\tau\in\mathbb{R}}p_S(\tau)\leqslant\frac{M_2}{w_\tau} \tag{3.26c}$$

for some constant $0<M_1<M_2<\infty$, and

$$\lim_{\Delta\tau\to0}\frac{\frac{d\mathcal{P}_S(\tau)}{d\tau}}{\Delta\tau}=\frac{dp_S(\tau)}{d\tau},\qquad \frac{dp_S(\tau)}{d\tau}=O\left(\frac{1}{w_\tau^2}\right) \tag{3.26d}$$

whenever the derivatives exist.

Remark 3.13 (i) It is rather complicated to conjecture general features of the distribution $\{\mathbb{P}_\xi^{(S,\tau)}\}$ because the crystal shape that chiefly affects the value of ξ_C may be to a large extent dependent on the experimental way of preparation of the electrode surface (see Remark 3.4(v)). This factor is often hard to take into account theoretically. Nevertheless, it turned out in our previous works [11, 12] that very good agreement of theoretical results with experiment could be achieved, even if ξ_C is taken constant.[9] On the other hand, it proved crucial to take into account variations in the crystal size S_C and the boundary tension $\tau_C^{\omega_E(C)}$.

(ii) Due to the immense number of crystals on the electrode surface, $|\mathcal{C}_E|\gg1$, the values $\tau\in\mathcal{T}_E$ are to be extremely closely spaced ($\Delta\tau\to0$) and the average $\langle\cdot\rangle_\tau$ is to be practically the same if the number of crystals is multiplied (macroscopic reproducibility). Viewing $\tau_C^{\omega_E(C)}$ as a *random boundary* quantity, almost all crystals should have the values of the

[9] In Appendix we briefly discuss the situation when the effect of the average $\langle\cdot\rangle_\xi$ is not completely overlooked.

boundary tension concentrated in an interval of length proportional to the inverse magnitude of fluctuations on the crystal boundary, i.e., proportional to $B_C^{-1/2} = \xi_C^{-1/2} S_C^{-1/4}$.

(iii) Since the area $\int p_S(\tau)\, d\tau$ of the function p_S is 1, the height of p_S is assumed to be of the order $O(\frac{1}{\operatorname{supp} p_S}) = O(\frac{1}{w_\tau})$. Then, similarly, the derivative of p_S is at most of the order $O(\frac{\sup_\tau p_S(\tau)}{\operatorname{supp} p_S}) = O(\frac{1}{w_\tau^2})$.

The assumption (As6) makes the average $\langle\cdot\rangle_\xi$ trivial to perform. Using (As7), the average $\langle\cdot\rangle_\tau$ can also be managed by finding the leading contribution and estimating the remaining ones. As a result, we express the $\langle\cdot\rangle_C$ average as an average over the sizes S of crystals of a dominant term and a remainder.

Statement 3.14 *Let* $0 < \delta < \frac{1}{8}$ *and let* (As1)–(As7) *be true. Introduce*

$$\tau_S(\psi) \equiv -\frac{4h\sqrt{S}}{a\xi_0}(\psi - \psi_{\mathrm{tr}}). \tag{3.27}$$

Then

$$J_E^{\omega_E}(\psi) = \langle \mathcal{D}_S(\psi) + \mathcal{R}_S^{\omega_E}(\psi)\rangle_S, \tag{3.28}$$

where

$$\mathcal{D}_S(\psi) \equiv \frac{4h}{\xi_0}\sqrt{S}\, p_S(\tau_S(\psi)) \tag{3.29}$$

with

$$\frac{M_1}{\bar{w}_2} S^{3/4} \leqslant \sup_\psi \mathcal{D}_S(\psi) \leqslant \frac{M_2}{\bar{w}_1} S^{3/4} \tag{3.30}$$

(*the constants* $\bar{w}_1$, $\bar{w}_2$, M_1, *and* M_2 *were introduced in* (As7)) *and the remainder*

$$|\mathcal{R}_S^{\omega_E}(\psi)| \leqslant \frac{4h}{\xi_0}\left[\frac{1}{\beta} O(S^{1/2+2\delta}) + O(S^{1/2}) + O(S^{3/4} e^{-2S^\delta})\right]. \tag{3.31}$$

The statement is verified in Sect. 5.

Remark 3.15 (i) Notice that $\tau_S(\psi)$ is the solution of the equation $\psi_C(S, \tau, \xi_0) = \psi$, where ψ_C was defined in (3.20). Thus, at $\tau = \tau_S(\psi)$ and $\xi = \xi_0$ the argument of $\cosh^{-2}$ in (3.22) vanishes.

(ii) Consider the function $j_C(S, \tau, \xi, \psi)$ that very well approximates the current density from a single crystal (see (3.21)). From (3.28) and (3.29) it follows that the τ-average $\langle j_C(S, \tau, \xi_0, \psi)\rangle_\tau$ can be well described by $\mathcal{D}_S(\psi)$ — a suitably re-scaled function p_S. Thus, the effect of the τ-average is to decrease the height of the $\cosh^{-2}$ spike exhibited by $j_C(S, \tau, \xi_0, \psi)$ from $O(S)$ to $O(S^{3/4})$ and, since the spike's area is essentially crystal independent (see (3.9)), to increase the spike's width from $O(S^{-1})$ to $O(S^{-3/4})$. The dominant term $\mathcal{D}_S(\psi)$ is concentrated around the potential ψ for which $\tau_S(\psi) = \tau_0$, i.e., around $\psi_C(S, \tau_0, \xi_0)$. Notice also that $\mathcal{D}_S(\psi)$ is β-independent, once $p_S(\tau)$ is so.

(iii) The heuristic idea behind the results of Statement 3.14 is as follows. When τ is changed, the profile of the spike exhibited by $j_C(S, \tau, \xi_0, \psi)$ remains the same, the spike

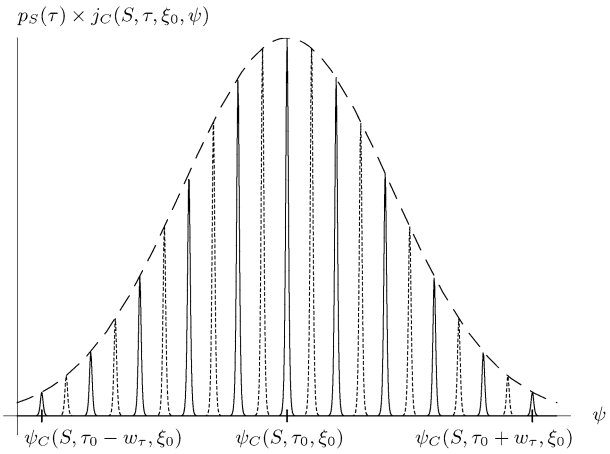

Fig. 1 The crystal current density $j_C(S, \tau, \xi_0, \psi)$ weighed with the Gaussian distribution $p_S(\tau)$ with S constant plotted for several equidistant values of τ (alternating *full and dotted lines*). The *dashed line* represents the corresponding average $\langle j_C(S, \tau, \xi_0, \psi)\rangle_\tau$ multiplied by a suitable constant to give the height of the central spike. The average $\langle j_C(S, \tau, \xi_0, \psi)\rangle_\tau$ is again Gaussian

(the maximum position $\psi_C(S, \tau, \xi_0)$) only gets shifted. According to (3.20), this shift is *proportional*, by the factor $\frac{a\xi_0}{4h\sqrt{S}}$, to the change of τ. Thus, as τ changes over the interval $[\tau_0 - w_\tau, \tau_0 + w_\tau]$ of length $2w_\tau = O(S^{-1/4})$, the spikes of $j_C(S, \tau, \xi_0, \psi)$ are spread, proportionally to τ, over an interval of length $2w_\tau \frac{a\xi_0}{4h\sqrt{S}} + O(S^{-1}) = O(S^{-3/4})$ (the term $O(S^{-1})$ represents the half-width of $j_C(S, \tau, \xi_0, \psi)$). Since the half-width $O(S^{-1})$ of the spikes is much less than the interval's width $O(S^{-3/4})$, the profile of the average $\langle j_C(S, \tau, \xi_0, \psi)\rangle_\tau$ is well approximated by the profile of p_S.

Constructing a lattice gas model, in Ref. [12] we obtained $p_S(\tau)$ that was a Gaussian centered at τ_0. Taking such $p_S(\tau)$, Fig. 1 shows an illustrative plot of the product $p_S(\tau) \times j_C(S, \tau, \xi_0, \psi)$ for several values of τ with S kept constant. The average $\langle j_C(S, \tau, \xi_0, \psi)\rangle_\tau \approx \mathcal{D}_S(\psi)$ is again (very precisely) Gaussian.

(iv) Experimental voltammogram spikes are almost always asymmetric. Considering a symmetric average $\langle j_C(S, \tau, \xi_0, \psi)\rangle_\tau$ such as the one from Fig. 1, it is easy to perceive that (3.28) predicts a current density $J_E^{\boldsymbol{\omega}_E}(\psi)$ that is typically asymmetric. Indeed, in view of (3.20), the point $\psi_C(S, \tau_0, \xi_0)$ around which the symmetric average $\langle j_C(S, \tau, \xi_0, \psi)\rangle_\tau$ is centered depends on S *non*-linearly. Then, as S varies, the points $\psi_C(S, \tau_0, \xi_0)$ *accumulate* at ψ_{tr} from one side (depending on the sign of τ_0), i.e., the spikes exhibited by $\langle j_C(S, \tau, \xi_0, \psi)\rangle_\tau$ are spread *in*homogeneously on the ψ-axes (see Fig. 2). Then $J_E^{\boldsymbol{\omega}_E}(\psi)$, the average of these spikes over S, is in general asymmetric, even if the distribution $\{\mathbb{P}_S\}$ is symmetric (see Fig. 3). The only case when $J_E^{\boldsymbol{\omega}_E}(\psi)$ is symmetric corresponds in the considered situation to $\tau_0 = 0$ when there are no shifts between various spikes, $\psi_C(S, \tau_0 = 0, \xi_0) = \mathrm{const} = \psi_{\mathrm{tr}}$ (see also Remark 4.2(vi)).

4 Application to Experiment

For application purposes, it is convenient to know global features of the electrode current density $J_E^{\boldsymbol{\omega}_E}(\psi)$, such as its maximum position, height, or asymmetry. In principle, these can be derived from the bound (3.28), or at least within the approximation

$$J_E^{\boldsymbol{\omega}_E}(\psi) \approx \langle \mathcal{D}_S(\psi)\rangle_S \tag{4.1}$$

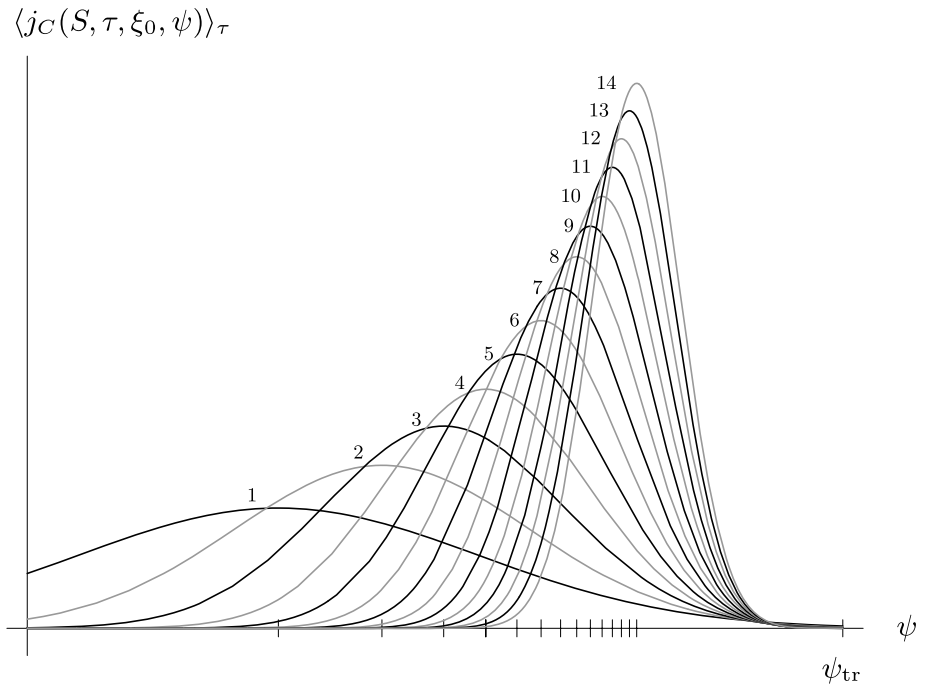

Fig. 2 The averages $\langle j_C(S,\tau,\xi_0,\psi)\rangle_\tau$ for $S = 1,\dots,14$ depicted as Gaussians. For each spike its maximum point $\psi_C(S,\tau_0,\xi_0)$, where $\tau_0 > 0$ is fixed, is indicated on the ψ-axes. As S increases, the maximum positions accumulate from the left at ψ_{tr}

of the dominant term $\mathcal{D}_S(\psi)$ from (3.28), provided a more detailed knowledge of the function $p_S(\tau)$ from (As7)(c) and of the distribution $\mathbb{P}_S$ of crystal sizes is available.

We will not pursue the task on a general level — this would require the adoption of further assumptions on the behavior of $p_S(\tau)$ and $\mathbb{P}_S$. Instead, in order to obtain results that can be readily applied to experiments, we will consider a specific, simple example of the function $p_S(\tau)$. Namely, we let the function be of a triangular shape that is symmetric around τ_0 and independent of the crystal size S,

$$p_S(\tau) = \Delta(\tau) \equiv \begin{cases} \frac{S_0^{1/4}}{\delta}\big(1 - \frac{S_0^{1/4}}{\delta}|\tau - \tau_0|\big), & |\tau - \tau_0| \leqslant \frac{\delta}{S_0^{1/4}}, \\ 0, & |\tau - \tau_0| \geqslant \frac{\delta}{S_0^{1/4}}, \end{cases} \tag{4.2}$$

where S_0 is a fixed crystal size and the parameter $\delta > 0$. The ratio $\frac{\delta}{S_0^{1/4}}$ is the half-width of the function $\Delta(\tau)$. In addition, we will approximate the discrete average over the crystal sizes S by a continuous one, i.e., we consider a continuous probability density function $\rho(S)$ such that

$$\langle\cdot\rangle_S \approx \int_0^\infty \cdot\,\rho(S)\,dS; \tag{4.3}$$

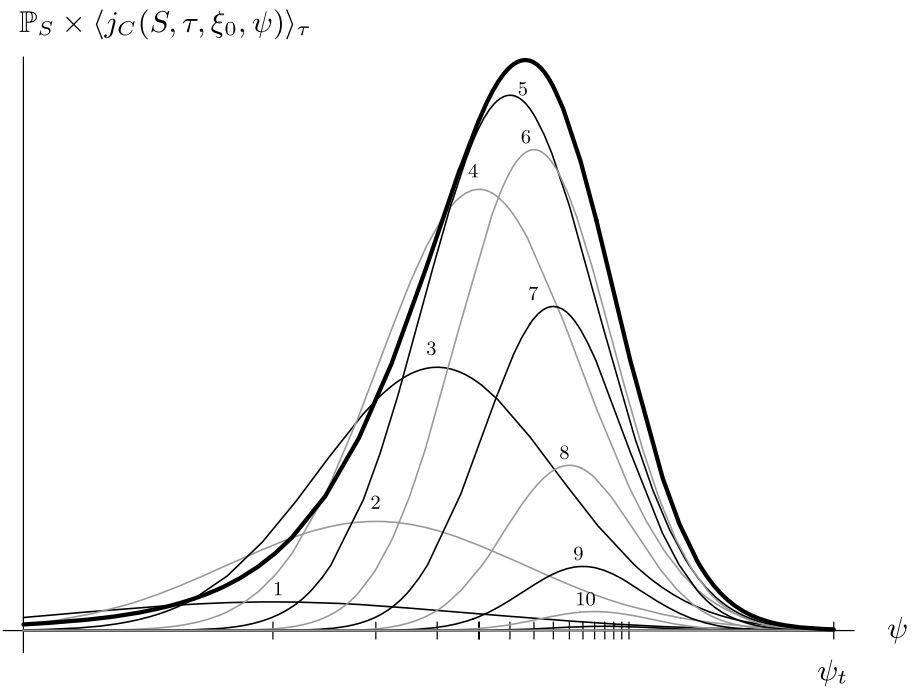

Fig. 3 The averages $\langle j_C(S,\tau,\xi_0,\psi)\rangle_\tau$ from Fig. 2 weighed with a Gaussian distribution $\mathbb{P}_S$ plotted for $S = 1,\ldots,14$ (the averages for $S > 10$ practically vanish). The thick spike is the resulting current density $J_E^{\boldsymbol{\omega}_E}(\psi)$ multiplied by a suitable constant to fit the plot

this will simplify the forthcoming analysis (see Lemma 6.3 and 6.1). Hence, combining (4.1), (4.2), and (4.3), we have

$$J_E^{\boldsymbol{\omega}_E}(\psi) \approx \mathcal{J}(\psi - \psi_{\mathrm{tr}}) \tag{4.4}$$

with

$$\mathcal{J}(x) \equiv \frac{4h}{\xi_0}\int_0^\infty \Delta\left(-\frac{4h\sqrt{S}}{a\xi_0}x\right)\sqrt{S}\rho(S)\,dS. \tag{4.5}$$

Statement 4.1 *Let $\rho : [0,\infty) \to [0,\infty)$ be a continuous probability density function with a support $(0, S_\rho)$, where $0 < S_\rho \leqslant S_{\mathrm{tot}}$.*[10]

(1) *The function $\mathcal{J}$ evaluated for τ_0 and for $-\tau_0$ are reflections of each other,*

$$[\mathcal{J}(x)]_{\tau_0} = [\mathcal{J}(-x)]_{-\tau_0}. \tag{4.6}$$

(2) *The function $\mathcal{J}$ attains a maximum at $x = x_{\max}$ if and only if*

$$x_{\max} = -\frac{a\xi_0\tau_0}{4h\sqrt{S_{\max}}}, \tag{4.7}$$

[10]The crystal size cannot exceed the total number $S_{\mathrm{tot}} < \infty$ of the adsorption sites on the electrode surface.

where the crystal size $0 < S_{\max} < S_\rho$ *is the solution of the equation*

$$\int_{S_1}^{S_{\max}} S\rho(S)\,dS = \int_{S_{\max}}^{S_2} S\rho(S)\,dS, \tag{4.8}$$

and satisfies the inequality

$$2S_{\max}^2\rho(S_{\max}) > S_1^2\rho(S_1) + S_2^2\rho(S_2). \tag{4.9}$$

Here

$$S_1 \equiv \begin{cases} (1-\frac{1}{|c|})^2 S_{\max}, & |c| \geqslant 1, \\ 0, & |c| \leqslant 1, \end{cases} \qquad S_2 \equiv \left(1+\frac{1}{|c|}\right)^2 S_{\max}, \quad c \equiv \frac{\tau_0 S_0^{1/4}}{\delta}. \tag{4.10}$$

(3) *The maximal value*

$$H \equiv \mathcal{J}(x_{\max}) = \frac{4hS_0^{1/4}}{\xi_0\delta} H_0, \tag{4.11}$$

where

$$H_0 \equiv \int_{S_1}^{S_2} (1-|x_S|)\sqrt{S}\rho(S)\,dS \quad \text{with } x_S \equiv c\left(\sqrt{\frac{S}{S_{\max}}} - 1\right). \tag{4.12}$$

(4) *The area*

$$A \equiv \int_{\mathbb{R}} \mathcal{J}(x)\,dx = a \tag{4.13}$$

and the ratio of the area to the left of $x_{\max}$ *and the total area*

$$\alpha \equiv \frac{1}{A}\int_{-\infty}^{x_{\max}} \mathcal{J}(x)\,dx = \int_{S_1}^{S_2} \frac{1 - x_S(2-|x_S|)}{2}\rho(S)\,dS + \alpha_0 \tag{4.14}$$

where

$$\alpha_0 \equiv \begin{cases} \int_0^{S_1} \rho(S)\,dS, & \tau_0 \geqslant 0, \\ \int_{S_2}^{\infty} \rho(S)\,dS, & \tau_0 \leqslant 0. \end{cases} \tag{4.15}$$

Statement 4.1 is verified in Sect. 6.

Remark 4.2 (i) As a matter of fact, Statement 4.1(1) is, within the approximation (4.1), true also for the current density $J_E^{\omega_E}$ as soon as $p_S(\tau)$ is *symmetric* around τ_0 (not necessarily of a triangular shape). In addition, it is equally valid for discrete and continuous distributions of the crystal sizes S.

(ii) Statement 4.1(1) implies

$$(x_{\max})_{\tau_0} = -(x_{\max})_{-\tau_0}, \qquad (H)_{\tau_0} = H_{-\tau_0}, \qquad (\alpha)_{\tau_0} = 1 - (\alpha)_{-\tau_0}. \tag{4.16}$$

It is easy to check that (4.7), (4.11), and (4.14) satisfy these symmetry relations. The physical difference between the cases $\tau_0 > 0$ and $\tau_0 < 0$ is that boundary conditions prefer the phase $+$ in the former case and the phase $-$ in the latter case (see (3.4) and the end of Remark 2.9). Consequently, the maximum $x_{\max}$ is shifted below and above zero, respectively.

(iii) The equation (4.8) says that the areas of the function $S\rho(S)$ within the intervals $S_1 \leqslant S \leqslant S_{\max}$ and $S_{\max} \leqslant S \leqslant S_2$, respectively, coincide.

(iv) The equality (4.13) remains true even within the approximation (4.1),

$$\left\langle \int_{\mathbb{R}} \mathcal{D}_S(x)\,dx \right\rangle_S = \frac{4h}{\xi_0} \left\langle \sqrt{S} \int_{\mathbb{R}} p_S(\tau_S(x))\,dx \right\rangle_S = a \left\langle \int_{\mathbb{R}} p_S(\tau)\,d\tau \right\rangle_S = a. \tag{4.17}$$

(v) The parameter α characterizes an asymmetry of the function $\mathcal{J}$. The extremal values of α correspond to the limits $\tau_0 \to \pm\infty$ ("infinitely large" shifts between the spikes exhibited by $\Delta(-\frac{4h\sqrt{S}}{a\xi_0}x)$). In Sect. 6 we show that the extremal values are

$$\alpha_{\max} \equiv \lim_{\tau_0 \to \infty} \alpha = \int_0^{S_{\max}^{\infty}} \rho(S)\,dS, \qquad \alpha_{\min} \equiv \lim_{\tau_0 \to -\infty} \alpha = \int_{S_{\max}^{\infty}}^{\infty} \rho(S)\,dS, \tag{4.18}$$

where $S_{\max}^{\infty} \equiv \lim_{|c|\to\infty} S_{\max}(c)$. Moreover, if $\rho(S)$ is sufficiently differentiable, then $S_{\max}^{\infty}$ can be approximated by the maximum $\tilde{S}_{\max}^{\infty}$ of the function $S^{3/2}\rho(S)$ (i.e., $\frac{d[S^{3/2}\rho(S)]}{dS} = 0$ and $\frac{d^2[S^{3/2}\rho(S)]}{dS^2} < 0$ at $S = \tilde{S}_{\max}^{\infty}$).

(vi) In particular, if $\tau_0 = 0$, then we have

$$x_{\max} = 0, \qquad H = \frac{4hS_0^{1/4}}{\xi_0\delta} \int_0^{\infty} \sqrt{S}\rho(S)\,dS, \qquad \alpha = \frac{1}{2}, \tag{4.19}$$

i.e., the function $\mathcal{J}(x)$ is symmetric around its unique maximum attained at $x = 0$. Physically, the value $\tau_0 = 0$ corresponds to "neutral" boundary conditions — the situation when the boundary conditions do not prefer either of the two phases in the system. As a consequence, the maximum position $x_C(S, \tau_0 = 0, \xi_0) = 0$ of the function $\Delta(\tau_S(x))$ is the *same* for every S, i.e., the symmetric spikes exhibited by the function are *not* mutually shifted. We derived (4.19) in Ref. [11] for the special case of the Ising model (used there to describe the underpotential deposition of Cu on Pt(111)).

4.1 Two Examples

In order that Statement 4.1 can be applied, it is necessary to know the probability density function $\rho(S)$. In this subsection we consider two simple examples of the function $\rho(S)$ for which we explore the results of Statement 4.1.

4.1.1 Example 1

Let us assume that the distribution of crystals on the electrode surface that are of size S is the Gaussian $\tilde{\rho}_G(S)$ with the mean value $S_G > 0$ and the variance $\frac{S_G^2}{2\pi}$. Then the distribution of adsorption sites lying in crystals of size S is

$$\rho_G(S) \equiv \frac{S\tilde{\rho}_G(S)}{\int_0^{\infty} S\tilde{\rho}_G(S)\,dS} = (1 - \epsilon_G)\frac{S}{S_G^2} e^{-\pi(\frac{S}{S_G}-1)^2}, \tag{4.20}$$

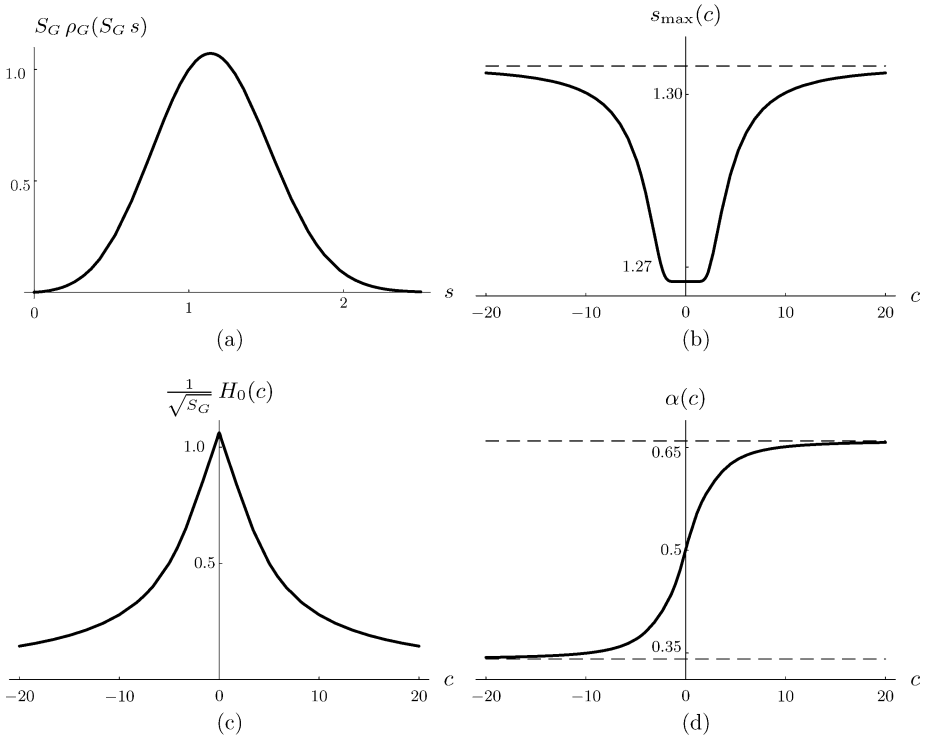

Fig. 4 The results of Statement 4.1 exemplified for the probability density function $\rho_G(S)$ from (4.20). The function $S_G\rho_G(S_G s) = (1-\epsilon_G)se^{-\pi(s-1)^2}$ is show in (**a**)

where $\epsilon_G \equiv \frac{e^{-\pi}+\pi\,\mathrm{erf}\sqrt{\pi}-\pi}{e^{-\pi}+\pi\,\mathrm{erf}\sqrt{\pi}+\pi} \doteq 7.82710^{-4}$. Strictly speaking, the support of $\rho_G(S)$ is the infinite interval $(0,\infty)$ and not only a finite interval $(0, S_\rho)$. Nevertheless, due to the exponential decay, this fact may be neglected for practical applications.

Applying Statement 4.1 to ρ_G, we readily get the following results.

(1) The crystal size $S_{\max} = \frac{s_{\max}}{S_G}$, where $s_{\max}$ is the solution of the equation

$$\left(\int_{s_1}^{s_{\max}} - \int_{s_{\max}}^{s_2}\right) s^2 e^{-\pi(s-1)^2}\,ds = 0 \tag{4.21}$$

with

$$s_1 \equiv \begin{cases} (1-\frac{1}{|c|})^2 s_{\max}, & |c| \geqslant 1, \\ 0, & |c| \leqslant 1, \end{cases} \qquad s_2 \equiv \left(1+\frac{1}{|c|}\right)^2 s_{\max}. \tag{4.22}$$

(2) The maximal value

$$H = \frac{4hS_0^{1/4}}{\xi_0\delta} H_0, \tag{4.23}$$

where

$$H_0 \equiv \sqrt{S_G}\int_{s_1}^{s_2}(1-|X_s|)s^{3/2}e^{-\pi(s-1)^2}\,ds \quad \text{with } X_s \equiv c\left(\sqrt{\frac{s}{s_{\max}}}-1\right). \tag{4.24}$$

(3) The ratio

$$\alpha = \int_{s_1}^{s_2}\frac{1-X_s(2-|X_s|)}{2}se^{-\pi(s-1)^2}\,ds + \begin{cases}\int_0^{s_1} se^{-\pi(s-1)^2}\,ds, & \tau_0 \geqslant 0,\\ \int_{s_2}^{\infty} se^{-\pi(s-1)^2}\,ds, & \tau_0 \leqslant 0.\end{cases} \tag{4.25}$$

Fig. 4 shows the dependencies of $s_{\max}$, H_0, and α on the parameter c as evaluated for the density function $\rho_G(S)$. Notice that, using Remark 4.2(v) and (4.11), we have

$$\begin{aligned} &s_{\max}(c=\pm\infty) \approx \frac{1+\sqrt{1+\frac{5}{\pi}}}{2} \doteq 1.305,\\ &\alpha_{\max} \doteq 0.660, \qquad \alpha_{\min} \doteq 0.341,\\ &\frac{1}{\sqrt{S_G}}H_0(0) = \int_0^{\infty} s^{3/2}e^{-\pi(s-1)^2}\,ds \doteq 1.062. \end{aligned} \tag{4.26}$$

4.1.2 Example 2

As another example, we consider the distribution that we introduced in Refs. [11, 12]. Namely, supposing that the crystals are a result of line defects occurring with a probability $0 < P < 1$, the distribution $\tilde{\rho}_H(S)$ of crystal sizes on the electrode surface is proportional to $(1-P)^{B_C/2} = (1-P)^{\xi_0\sqrt{S}/2}$, where we recalled (As6). Therefore, using the shorthand

$$S_H \equiv \left[\frac{2}{\xi_0\log(1-P)}\right]^2, \tag{4.27}$$

we have $\tilde{\rho}_H(S) = \frac{1}{2S_H}e^{-\sqrt{S/S_H}}$, implying

$$\rho_H(S) \equiv \frac{S\tilde{\rho}_H(S)}{\int_0^{\infty} S\tilde{\rho}_H(S)\,dS} = \frac{S}{12S_H^2}e^{-\sqrt{S/S_H}}, \quad S_H > 0. \tag{4.28}$$

Again, due to the exponential decay, one may neglect for practical applications that the support of $\rho_H(S)$ is the infinite interval $(0,\infty)$ instead of a finite interval $(0, S_\rho)$.

Applying Statement 4.1 to ρ_H, we obtain these results.

(1) The crystal size $S_{\max} = \frac{s_{\max}}{S_G}$, where $s_{\max}$ is the solution of the equation

$$\left(\int_{s_1}^{s_{\max}} - \int_{s_{\max}}^{s_2}\right)s^2e^{-\sqrt{s}}\,ds = 0 \tag{4.29}$$

with s_1, s_2 defined by (4.22).

(2) The maximal value

$$H = \frac{4hS_0^{1/4}}{\xi_0\delta}H_0, \tag{4.30}$$

where

$$H_0 \equiv \frac{\sqrt{S_H}}{12} \int_{s_1}^{s_2} (1 - |X_s|) s^{3/2} e^{-\sqrt{s}}\, ds, \tag{4.31}$$

with X_s defined in (4.24).

(3) The ratio

$$\alpha = \frac{1}{12} \int_{s_1}^{s_2} \frac{1 - X_s(2 - |X_s|)}{2} s e^{-\sqrt{s}}\, ds + \frac{1}{12} \times \begin{cases} \int_0^{s_1} s e^{-\sqrt{s}}\, ds, & \tau_0 \geqslant 0, \\ \int_{s_2}^{\infty} s e^{-\sqrt{s}}\, ds, & \tau_0 \leqslant 0. \end{cases} \tag{4.32}$$

Figure 5 shows the dependencies of $s_{\max}$, H_0, and α on the parameter c as evaluated for the density function $\rho_H(S)$. Notice that, using Remark 4.2(iv) and (4.11), we have

$$\begin{aligned} &s_{\max}(c = \pm\infty) \approx 25, \\ &\alpha_{\max} \approx 1 - \frac{118}{3e^5} \doteq 0.735, \qquad \alpha_{\min} \approx \frac{118}{3e^5} \doteq 0.265, \\ &\frac{1}{\sqrt{S_H}} H_0(0) = \int_0^{\infty} s^{3/2} e^{-\sqrt{s}}\, ds = 4. \end{aligned} \tag{4.33}$$

4.2 Microscopic Interpretation

A statistical mechanical lattice gas model can be used to microscopically simulate phase transitions on the electrode surface. For the sake of illustration, let us consider the simple case of a voltammogram spike that is associated with the first-order phase transition that occurs when the ion adsorbed on the electrode surface discharges and forms a full monolayer ($\theta(\infty) - \theta(-\infty) = 1$) on the surface.

Namely, we consider the standard, one-component lattice gas on the lattice $\mathcal{L}$ with an attractive nearest-neighbor interaction $\epsilon < 0$, the corresponding Hamiltonian in a crystal C being

$$H_C^{\omega}(\boldsymbol{\sigma}) = \epsilon N_C^{(2)}(\boldsymbol{\sigma}) - \mu N_C^{(1)}(\boldsymbol{\sigma}) + \omega \mathcal{N}_C^{(2)}(\boldsymbol{\sigma}). \tag{4.34}$$

At any site $x \in C$ either $\boldsymbol{\sigma}_x = 1$ or $\boldsymbol{\sigma}_x = 0$ (the site is either occupied by the deposited ion or it is vacant), $N_C^{(1)}(\boldsymbol{\sigma})$ is the number of sites in the crystal occupied in $\boldsymbol{\sigma}$, $N_C^{(2)}(\boldsymbol{\sigma})$ is the number of nearest-neighbor pairs of sites in C both of which are occupied in $\boldsymbol{\sigma}$, and $\mathcal{N}_C^{(2)}(\boldsymbol{\sigma})$ is the number of nearest-neighbor pairs of sites one site of which is in C and is occupied in $\boldsymbol{\sigma}$ and the other site is outside the crystal. Thus, we assume fixed occupied boundary conditions $\boldsymbol{\omega}$ outside the crystal, but with an attractive interaction $\omega < 0$ that is in general different from the bulk interaction ϵ.

Whenever $|\epsilon|$ is sufficiently large and $\mu = \mu_{\mathrm{tr}} \equiv \frac{n_{\mathcal{L}}\epsilon}{2}$, the lattice gas model from (4.34) is known to exhibit a first-order phase transition at which the fully occupied phase coexists with the fully vacant one (see Sect. 5.3 in Ref. [25] and references therein). This model is therefore suitable for describing the considered phase transition.

Remark 4.3 The model from (4.34) is equivalent to the standard Ising model with the bulk coupling $-\frac{\epsilon}{4}$, the boundary coupling $-\frac{2\omega-\epsilon}{4}$, and the magnetic field $\frac{2\mu - n_{\mathcal{L}}\epsilon}{4}$ (see Ref. [11]). The value $\omega = \frac{\epsilon}{2}$ represents free boundary conditions. The "weak" boundary conditions (see Remark 2.7(i)) corresponds to ω such that $|\frac{\omega}{\epsilon} - \frac{1}{2}| \lesssim \frac{1}{6}$ [11].

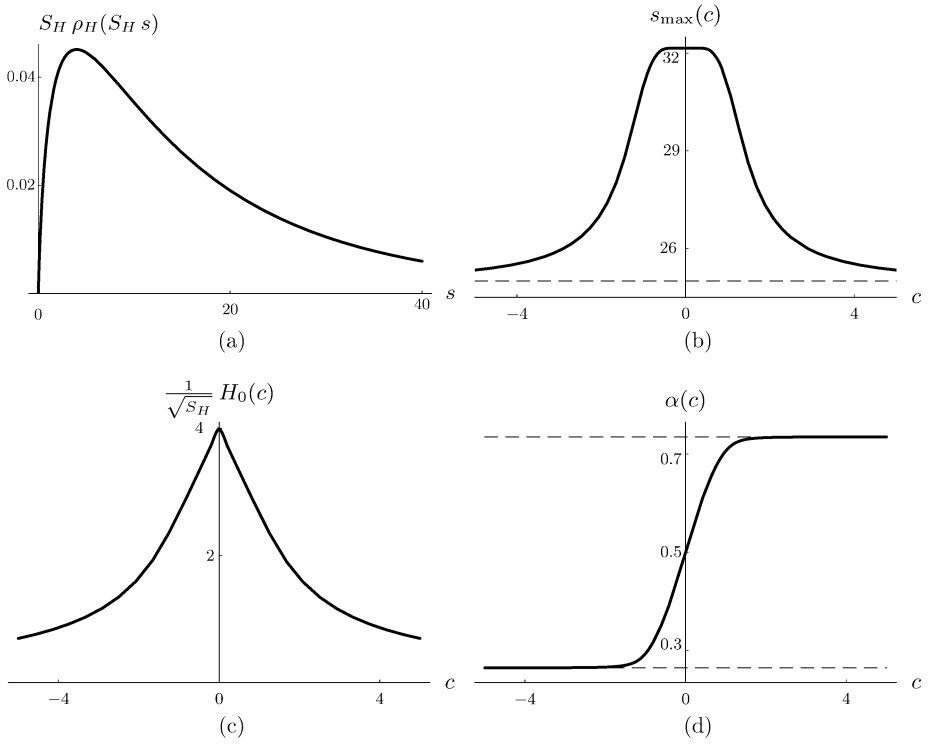

Fig. 5 The results of Statement 4.1 exemplified for the probability density function $\rho_H(S)$ from (4.28). The function $S_H\rho_H(S_H s) = \frac{s}{12}e^{-\sqrt{s}}$ is show in (**a**)

Observing that

$$\frac{n_{\mathcal{L}}}{2}(S_C - B_C) + \sum_{m=1}^{n_{\mathcal{L}}-1}\frac{m}{2}B_C^{(m)} \quad \text{and} \quad \sum_{m=1}^{n_{\mathcal{L}}-1}(n_{\mathcal{L}} - m)B_C^{(m)} \tag{4.35}$$

is the number of nearest-neighbor pairs inside C and the number of nearest-neighbor pairs with one site in C and the other one outside C, respectively, the energy of the fully occupied ground state in C is

$$E_+^{\omega}(C,\mu) = \frac{\epsilon n_{\mathcal{L}} - 2\mu}{2}S_C + \frac{2\omega - \epsilon}{2}\sum_{m=1}^{n_{\mathcal{L}}-1}(n_{\mathcal{L}} - m)B_C^{(m)}, \tag{4.36}$$

whereas the energy of the fully vacant ground state is

$$E_-^{\omega}(C,\mu) = 0, \tag{4.37}$$

implying

$$\begin{aligned} &e_+(\mu) = \frac{\epsilon n_{\mathcal{L}} - 2\mu}{2}, \qquad e_+^{\omega}(m,\mu) = \frac{2\omega - \epsilon}{2}(n_{\mathcal{L}} - m), \\ &e_-(\mu) = 0, \qquad e_-^{\omega}(m,\mu) = 0. \end{aligned} \tag{4.38}$$

4.2.1 The Dependence of τ_0 and δ on ϵ and ω

The parameters τ_0 and δ in the definition (4.2) of the function $\Delta(\tau)$ are connected with the interactions ϵ and ω of the lattice gas model (4.34). This becomes clear if one investigates the boundary conditions in a given crystal from the microscopic point of view. We provided such an analysis in Ref. [12]. The basic idea, tailored here to the model (4.34), is as follows.

Since boundary conditions are determined by the various defects surrounding the crystals formed on the electrode surface, physically most appropriate boundary conditions should be random. Then the average

$$\langle g_C(\tau)\rangle_\tau = \int g_C(\tau)\Delta(\tau)\,d\tau \tag{4.39}$$

of a function $g_C(\tau)$ over the values of τ_C^ω for the model (4.34) corresponds to the average over the randomness surrounding a given crystal. However, an essentially equivalent average result is to be obtained if the boundary conditions are fixed with an interaction ω that, although being constant along the boundary of every crystal, has values changing from crystal to crystal. The τ-average (4.39) is in this way replaced by the average over the various values of ω. Writing the value of ω for a given crystal C as proportional to the bulk interaction, $\omega = \eta\epsilon$, the average over ω becomes equivalent to the average over η, and we conclude

$$\int g_C(\tau)\Delta(\tau)\,d\tau \approx \int g_C(\tau_C^{\eta\epsilon})G(\eta)\,d\eta, \tag{4.40}$$

where $G(\eta)$ is the probability density function for the variable η. The relation (4.40) enables one to link τ_0 and δ to ϵ and ω as soon as $G(\eta)$ is known.

In order to describe $G(\eta)$, we identify η with the occupancy of the deposited ion in the region of defects around C, i.e., the number of sites along the outer boundary of C occupied by the ion divided by the number B_C of all outer boundary sites. Referring to the local-limit theorem, $G(\eta)$ may be approximated by the Gaussian probability density function $G_S(\eta)$ that has a mean value $0 < \eta_0 < 1$ and the variance [12]

$$D_S^2 = \frac{\eta_0(1-\eta_0)}{B_C} = \frac{\eta_0(1-\eta_0)}{\xi_0\sqrt{S}}.$$

In the last step we recalled that $B_C = \xi_0\sqrt{S_C}$.

In view of (2.17), (3.3), (3.5), and (4.38), we have

$$\tau_C^{\eta\epsilon} = u_C\eta + v_C \tag{4.41}$$

with

$$\begin{aligned} u_C &\equiv \left[\epsilon\sum_{m=1}^{n_{\mathcal{L}}-1}(n_{\mathcal{L}}-m)\frac{B_C^{(m)}}{B_C} + O(e^{-b\tilde{d}_0})\right]\left[1+O\left(\frac{1}{\sqrt{S_C}}\right)\right], \\ v_C &\equiv \left[-\frac{\epsilon}{2}\sum_{m=1}^{n_{\mathcal{L}}-1}(n_{\mathcal{L}}-m)\frac{B_C^{(m)}}{B_C} + O(e^{-b\tilde{d}_0})\right]\left[1+O\left(\frac{1}{\sqrt{S_C}}\right)\right]. \end{aligned} \tag{4.42}$$

Consequently,

$$\int g_C(\tau_C^{\eta\epsilon})G(\eta)\,d\eta \approx \int g(\tau)\frac{1}{|u_C|}G_S\left(\frac{\tau-v_C}{|u_C|}\right)d\tau. \tag{4.43}$$

Combined with (4.40), we require that the maximum position $u_C\eta_0 + v_C$ and the half-width $2\sqrt{\log 4}|u_C|D_{S_0}$ of $\frac{1}{|u_C|}G_{S_0}(\frac{\tau - v_C}{|u_C|})$ coincide with the maximum position τ_0 and the half-width $\frac{\delta}{S_0^{1/4}}$ of $\Delta(\tau)$. Hence, introducing $\omega_0 \equiv \eta_0\epsilon$, we find

$$\begin{aligned} \tau_0 &= u_C\frac{\omega_0}{\epsilon} + v_C, \\ \delta &= \frac{2|u_C|}{|\epsilon|}\left[\log 4\frac{\omega_0(\epsilon - \omega_0)}{\xi_0}\right]^{1/2} \quad (\epsilon < \omega_0 < 0). \end{aligned} \tag{4.44}$$

The quantities u_C and v_C are essentially independent of C for crystals of regular shapes when $B_C^{(m)}$ is either proportional to B_C or is constant with respect to B_C (the former terms $B_C^{(m)}$ are dominant, while the latter ones are negligible as $C \nearrow \mathcal{L}$). For example,

$$u_C \approx 2\epsilon, \qquad v_C \approx -\epsilon \quad \text{for a triangular } \mathcal{L} \text{ and } C \text{ parallelogram} \tag{4.45}$$

and

$$u_C \approx \epsilon, \qquad v_C \approx -\frac{\epsilon}{2} \quad \text{for a square } \mathcal{L} \text{ and } C \text{ square.} \tag{4.46}$$

4.3 How to Apply the Theory

The parameters occurring in our theory may be summarized as follows.

(a) *The macroscopic parameters to be taken from experiment:*

$$\psi_{\max}, \quad H, \quad A, \quad \alpha, \quad \kappa, \quad \nu, \quad \beta, \quad \theta_+^{\mathrm{tr}} - \theta_-^{\mathrm{tr}}.$$

Notice that the inverse temperature β is insignificant, for $J_E^{\omega_E}(\psi)$ is essentially independent of it (see Remark 3.15(ii) and (4.2)).

(b) *The parameters whose values can be evaluated from the theory.* Since only the first four parameters in (a) actually characterize the profile of a particular voltammogram spike, our theory can yield, for a given spike, the values of four parameters. We prefer these parameters to be

$$\gamma, \quad \psi_{\mathrm{tr}}, \quad \tau_0, \quad \delta.$$

The values of τ_0 and δ allow us to evaluate the corresponding values of the microscopic interactions ϵ and ω_0 for the model (4.34) via (4.44). Moreover, using that $\mu_{\mathrm{tr}} = -e_0\gamma(\psi_{\mathrm{tr}} - \psi_0)$ by (2.7) and that $\mu_{\mathrm{tr}} \equiv \frac{n_C\epsilon}{2}$, we obtain the value of the reference potential ψ_0.

(c) *The parameters whose values are to be chosen:*

$$\xi_0, \quad S_0, \quad \text{and the parameters in the definition of } \rho(S).$$

For instance, the parameters in the definition of the probability density functions $\rho_G(S)$ and $\rho_H(S)$ are S_G and S_H, respectively (see (4.20) and (4.28)).

Here is the sequence of steps for obtaining the values of γ, ψ_{tr}, τ_0, and δ from the experimentally measured values of A, $\psi_{\max}$, H, and α:

(1) find the function $S_{\max}(c)$ from (4.8);
(2) evaluate c, using (4.14) for the ratio α;

Table 1 The parameters appearing in the theory and their values obtained by fitting the theoretical voltammogram to experiment

Parameter	Type	Definition	Pt(111), [26]	Pt(100), [27]	Pt(100), [28]	Units
A	taken from	(4.13)	0.498	4.831	2.567	μA V cm^{-2}
$\psi_{\max}$	experiment	(4.7)	0.3462	0.714	0.596	V
H		(4.11)	23.35	186.3	116.8	μA cm^{-2}
α		(4.14)	0.502	0.709	0.670	
κe_0		(1.2)	241.1	208.8	208.8	μC cm^{-2}
ν		(1.2)	1.0	20.0	10.0	mV s^{-1}
βe_0		$e_0/(k_B T)$	38.92	38.92	38.92	V^{-1}
$\theta_+^{\mathrm{tr}} - \theta_-^{\mathrm{tr}}$		(3.1)	1.0	1.0	1.0	
ξ_0	chosen	(As6)	4.0	4.0	4.0	
$\rho(S)$		(4.3)	$S_G = 160.0$	$S_H = 22.52$	$S_H = 22.52$	
S_0		(4.2)	160.0	135.1	135.1	
γ	yielded by	(1.2)	2.066	1.157	1.229	
ψ_{tr}	theory	(2.24)	0.3468	0.727	0.605	V
τ_0		(As7)	4.229	96.21	70.23	meV
δ		(4.2)	525.4	319.2	330.8	meV^{-1}
ϵ		(4.34)	−446.3	−575.3	−579.2	meV
ω_0		(4.44)	−221.0	−191.4	−219.4	meV
ψ_0		(2.7)	−0.301	−0.268	−0.338	V

(3) evaluate $S_{\max}$ for this value of c;
(4) evaluate δ, using (4.11) for the height H;
(5) evaluate τ_0, using the definition of c from (4.10);
(6) evaluate ψ_{tr}, using (4.7) for the maximum position $\psi_{\max}$.

Independently, one can evaluate γ from (3.2) and (4.13) for the area A. Using thus obtained values of γ, ψ_{tr}, τ_0, and δ, we can evaluate the current density $J_E^{\omega_E}(\psi)$ from (4.4) and (4.5).

We illustrate the application of our theory to experiment with a voltammogram spike corresponding to the first-order phase transition that take place when the ion adsorbed on the electrode surface discharges and forms a full monolayer on the surface. This simple case can be microscopically simulated by the model (4.34).

4.3.1 Illustration 1

First, we consider a voltammogram spike with a small asymmetry (α is close to $\frac{1}{2}$). Then a good match with experiment may be expected even if the probability density function $\rho(S)$ is rather symmetric, and we take $\rho(S) = \rho_G(S)$ (see (4.20)). As an example, we use the spike measured in the underpotential deposition of Cu on Pt(111) from Ref. [26], Fig. 3(a). In this case the adsorption sites on the Pt electrode surface form a triangular lattice, the (commensurate) adsorbed Cu monolayer has a Cu–Cu distance of 2.77 Å [29], and we assume the crystals have the shape of a parallelogram. Column 4 in Table 1 contains the corresponding values of experimental parameters, the chosen values of the parameters ξ_0, S_0, and S_H, and the values of the parameters evaluated from the theory. Notice that we set S_0 equal to the

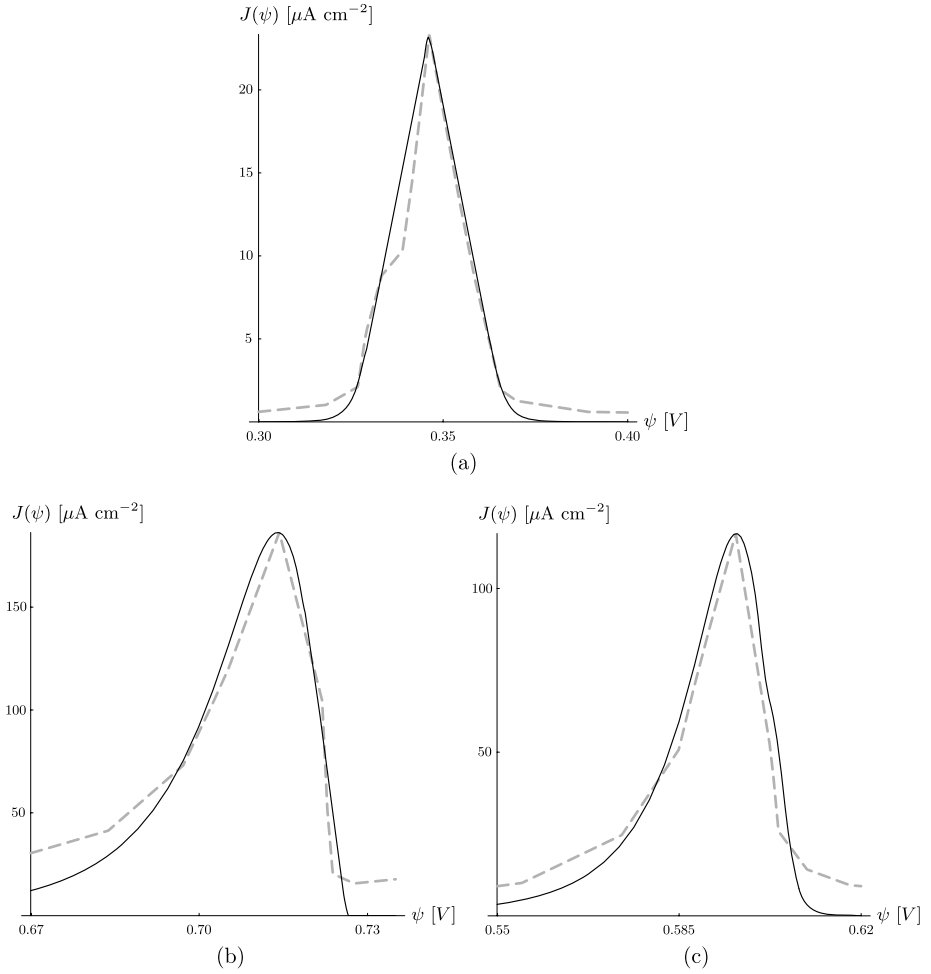

Fig. 6 Experimental voltammograms (*dashed lines*) compared to the theoretical fit (*full lines*)

mean size S_G of $\rho_G(S)$. The choice $S_G = 160$ amounts to the average linear crystal size, approximately $\sqrt{S_G} \doteq 12.65$. In Fig. 6(a) we show the comparison of the theoretical and the experimental voltammogram.

4.3.2 Illustration 2

Next, we consider a voltammogram spike with a moderate asymmetry, namely, the spike associated with the underpotential deposition of Cu on Pt(100) from Ref. [27], Fig. 1(a) and from Ref. [28], Fig 3(c). In this case the adsorption sites form a square lattice with the Cu–Cu distance of 2.77 Å in the adsorbed monolayer [27]. We assume the crystals have the shape of a square and take $\rho(S) = \rho_H(S)$ (see (4.28)). Columns 5 and 6 in Table 1 contain the corresponding respective values of the involved parameters. We set S_0 equal to the mean size $6S_H$ of $\rho_H(S)$. Choosing the line defect probability $P = \frac{1}{10}$ (see (4.27)), we have $S_H \doteq 22.52$, and the average linear crystal size is approximately $\sqrt{6S_H} \doteq 11.62$. Figures 6(b) and

6(c) show the theoretical and the experimental voltammograms. Their agreement is harder to achieve in the former case (Fig. 6(b)) because the ratio α is rather close to the maximal value $\alpha_{\max}$ (see (4.33)).

4.4 Concluding Remarks

We finish the section with remarks on two issues of interest.

4.4.1 Can a Voltammogram Spike Correspond to the Current Density from a Single Crystal?

It would be very natural to assume that a voltammogram spike is a result of a first-order phase transition in a single crystal C, i.e., $J_E^{\boldsymbol{\omega}E}(\psi) \approx j_C(S, \tau, \xi_0, \psi)$, where S and τ are some "typical" values of the crystal size and of the boundary tension, respectively.

However, in the three experiments considered in the previous subsection this interpretation is clearly wrong. Indeed, the height of the spike exhibited by $j_C(S, \tau, \xi_0, \psi)$ is approximately $\frac{a^2\beta S}{4\kappa\nu}$ (see (3.22) and (3.2)), while its half-width is about a divided by the height. Evaluating this height and half-width for the experimental values of a, β, κ, and ν from Table 1, they would match the height and the half-width of the voltammogram spike only if the crystal size is unrealistically small: $S \doteq 2$ (for the Pt(111) case) and $S \doteq 4$ (for the two Pt(100) cases). Equivalently, the spikes exhibited by the current density from a single, "typical" crystal with a realistic size (say, $S = 150$) are taller and narrower by a factor of about 50 or more than those measured in experiments.

In this way the height and the half-width of a voltammogram spike tell us about the structure of the electrode surface. Namely, whether the surface consists of a single crystal or many, essentially identical ("typical") crystals on the one hand, or whether the surface consists of many crystals with different sizes, boundary conditions, and shapes on the other one. In the former case the current density that would approximate a voltammogram spike can be obtained from a single crystal. In the latter case, however, the single-crystal interpretation of a voltammogram spike is completely erroneous, and one must consider the average from (3.18).

4.4.2 Comparison with Computer Simulated Studies

Rikvold and co-workers have intensively studied underpotential deposition with the help of computer simulations. As a specific example of first-order phase transitions, they considered the underpotential deposition of Cu on Au(111) [9]. Basically, their idea is to consider a particular lattice gas model on a crystal of a fixed size with periodic boundary conditions. Choosing suitable values of energetic interactions of the model, they try to fit the experimental spike, using numerical Monte Carlo simulations. They achieved very good qualitative agreement, the simulated spikes having the shape of those measured in experiments. However, the quantitative agreement is not completely satisfactory.

The philosophy of our theory is different. We assume that equilibrium statistical mechanics is applicable (i.e., experiments with relatively slow scan rates are considered). Shapes of voltammogram spikes are interpreted as averages, or "envelopes" of mutually shifted spikes of current densities coming from all the various crystals on the electrode surface. Once we can well control the *finite-size effects* that determine the single-crystal spikes, we eventually obtain a voltammogram spike. As a matter of fact, we can carry out the calculations analytically (with a certain number of rather simplifying, yet physically plausible approximations).

Since the finite-size effects in crystals show, under rather general conditions, a remarkable universality, one can work with "mesoscopic" quantities like τ_C^{ω} (see Statement 3.3), without ever referring to a specific lattice gas model. It is in terms of these quantities that we can actually fit a theoretical voltammogram spike to match an experimentally observed one. The values of the quantities used in the fit then lead to the values of energetic interactions in a lattice gas model, as soon as some model is constructed to simulate the deposition process. In this way, a voltammogram spike informs us *quantitatively* about microscopic behavior on the electrode surface, and our theory enables one to extract (at least a part of) this information.

It is still disputable which factors and to what extent they actually determine the broadening and asymmetry of voltammogram spikes. In many experiments, especially at higher potential scan rates, kinetic effects may be important (see the results of dynamic Monte Carlo simulations from Refs. [7, 8, 10]). Nevertheless, as pointed out in the Introduction, in the present paper we study only the stripping spikes so that kinetic effects should be less important than for the deposition spikes.

5 Verification of Statement 3.14

According to (3.21), (3.23), (3.4), and (3.13),

$$J_E^{\omega_E}(\psi) = h\beta\left\langle S\left\langle \cosh^{-2}\left[\frac{2h\beta S}{a}(\psi - \psi_C(S,\tau,\xi_0))\right]\right\rangle_\tau + O(\sqrt{S})\right\rangle_S$$

$$= h\beta\langle S\langle \cosh^{-2}[K_S(\tau - \tau_S(\psi))]\rangle_\tau + O(\sqrt{S})\rangle_S, \quad K_S \equiv \frac{\beta\xi_0\sqrt{S}}{2}, \tag{5.1}$$

where $\psi_C(S,\tau,\xi)$ and $\tau_S(\psi)$ were introduced in (3.20) and (3.27), respectively. Taking into account (3.19) and (3.26), we may write

$$\langle \cosh^{-2}[K_S(\tau - \tau_S)]\rangle_\tau = \sum_{\tau\in\mathcal{T}_E} \mathbb{P}_\tau^{(S)} \cosh^{-2}[K_S(\tau - \tau_S)]$$

$$= \sum_{\tau\in\mathcal{T}_E} \mathcal{P}_S(\tau) \cosh^{-2}[K_S(\tau - \tau_S)]$$

$$= \sum_{\tau\in\mathcal{T}_E^\infty} \mathcal{P}_S(\tau) \cosh^{-2}[K_S(\tau - \tau_S)] = X_1 + X_2, \tag{5.2}$$

where $\mathcal{T}_E^\infty$ is a partition of the real axis with a mesh size not exceeding $\Delta\tau$ such that $\mathcal{T}_E^\infty \cap [\tau_0 - w_\tau, \tau_0 + w_\tau] = \mathcal{T}_E$ and

$$X_1 \equiv \sum_{\tau\in\mathcal{T}_E^\infty} \frac{\mathcal{P}_S(\tau_S)}{\delta_\tau}\delta_\tau \cosh^{-2}[K_S(\tau - \tau_S)], \tag{5.3}$$

$$X_2 \equiv \left(\sum_{\substack{\tau\in\mathcal{T}_E^\infty:\\ K_S|\tau-\tau_S|\leqslant S^\delta}} + \sum_{\substack{\tau\in\mathcal{T}_E^\infty:\\ K_S|\tau-\tau_S|\geqslant S^\delta}}\right)\frac{\mathcal{P}_S(\tau) - \mathcal{P}_S(\tau_S)}{\delta_\tau}\delta_\tau \cosh^{-2}[K_S(\tau - \tau_S)]. \tag{5.4}$$

Here $0 < \delta_\tau \leqslant \Delta\tau$ is the distance between a given $\tau \in \mathcal{T}_E^\infty$ and the closest element $\tau' \in \mathcal{T}_E^\infty$ larger than τ. Clearly,

$$\lim_{\Delta\tau\to 0} X_1 = p_S(\tau_S)\int_{-\infty}^{\infty} \cosh^{-2}[K_S(\tau - \tau_S)]\,d\tau = \frac{2}{K_S}p_S(\tau_S). \tag{5.5}$$

Similarly,

$$\lim_{\Delta\tau\to 0} X_2 = \left(\int_{K_S|\tau-\tau_S|\leqslant S^\delta} + \int_{K_S|\tau-\tau_S|\geqslant S^\delta}\right)[p_S(\tau)-p_S(\tau_S)]\cosh^{-2}[K_S(\tau-\tau_S)]\,d\tau. \quad (5.6)$$

Using X_{21} to denote the first summand on the right-hand side of the last equation and X_{22} to denote the second one, we get

$$\begin{aligned} X_{21} &\leqslant \frac{2S^\delta}{K_S} \sup_{K_S|\tau-\tau_S|\geqslant S^\delta} |p_S(\tau)-p_S(\tau_S)| \leqslant \frac{2S^\delta}{K_S}\bar{p}'_S \sup_{K_S|\tau-\tau_S|\geqslant S^\delta} |\tau-\tau_S| \\ &\leqslant 2\bar{p}'_S\left(\frac{S^\delta}{K_S}\right)^2, \quad \bar{p}'_S \equiv \sup_\tau \left|\frac{dp_S(\tau)}{d\tau}\right|, \end{aligned} \quad (5.7)$$

where the last supremum is taken over all $\tau\in\mathbb{R}$ at which the derivative of p_S exists. Moreover, since $\cosh^{-2} x \leqslant 4e^{-2|x|}$ for all $x\in\mathbb{R}$, we get

$$\begin{aligned} X_{22} &\leqslant \sup_{\tau\in\mathbb{R}} |p_S(\tau)-p_S(\tau_S)| \int_{K_S|\tau-\tau_S|\geqslant S^\delta} 4e^{-2K_S|\tau-\tau_S|}\,d\tau \\ &\leqslant 4\bar{p}_S\frac{e^{-2S^\delta}}{K_S}, \quad \bar{p}_S \equiv \sup_\tau p_S(\tau). \end{aligned} \quad (5.8)$$

Combining the last two bounds with (5.1), (5.2), and (5.5), in the limit $\Delta\tau\to 0$ we arrive at the bound

$$\begin{aligned} J_E^{\omega_E}(\psi) &= h\beta\left\langle \frac{2S}{K_S}\left[p_S(\tau_S) + O\left(\bar{p}'_S\frac{S^{2\delta}}{K_S}\right) + O(\bar{p}_S e^{-2S^\delta})\right] + O(\sqrt{S})\right\rangle_S \\ &= \frac{4h}{\xi_0}\left\langle \sqrt{S}p_S(\tau_S) + \frac{1}{\beta}O(\bar{p}'_S S^{2\delta}) + O(\bar{p}_S\sqrt{S}e^{-2S^\delta}) + O(\sqrt{S})\right\rangle_S. \end{aligned} \quad (5.9)$$

Since $\bar{p}_S = O(S^{1/4})$ and $\bar{p}'_S = O(S^{1/2})$ by (As7), Statement 3.14 now follows.

6 Proof of Statement 4.1

6.1 Part (1)

Since only the function $\Delta(\tau)$ in the definition (4.5) of $\mathcal{J}(\psi)$ depends on τ_0 (see (4.2)), it suffices to observe that $\Delta(\tau)$ is symmetric around τ_0.

6.2 Part (2)

In the proof we will use two auxiliary lemmas, Lemma 6.1 and 6.3, that are stated below.

First, let $\tau_0 = 0$. Then, using (6.4) from Lemma 6.1 and the fact that $\rho(S) > 0$ for $0 < S < S_\rho$, we have $\frac{d\mathcal{J}(x)}{dx} > 0$ for every $x < 0$, whereas $\frac{d\mathcal{J}(x)}{dx} < 0$ for every $x > 0$. Consequently, $x_{\max} = 0$, and (4.7) is true (for any $S_{\max}$).

Second, let $\tau_0 > 0$. By virtue of Lemma 6.3 below,

$$\frac{d\mathcal{J}(x)}{dx} = \begin{cases} -a\left(\frac{u}{w}\right)^2 \int_0^{\left(\frac{\tau_0-w}{ux}\right)^2} S\rho(S)\,dS < 0, & \tau_0 < w, \\ 0, & \tau_0 \geqslant w, \end{cases} \quad \forall x \geqslant 0 \quad (6.1)$$

where $w \equiv \frac{\delta}{S_0^{1/4}} > 0$ and $u \equiv \frac{4h}{a\xi_0} > 0$. Moreover, in the case $\tau_0 \geqslant w$ and $x \geqslant 0$ we also have $\mathcal{J}(x) = 0$ because $-\frac{4h\sqrt{S}}{a\xi_0}x \leqslant 0 \leqslant \tau_0 - w$ so that $\Delta(-\frac{4h\sqrt{S}}{a\xi_0}x) = 0$ by definition. We therefore conclude that if $x_{\max}$ exists, it must be that $x_{\max} < 0$. Using now (6.14), we may express the conditions $\frac{d\mathcal{J}(x_{\max})}{dx} = 0$ and $\frac{d^2\mathcal{J}(x_{\max})}{dx^2} < 0$ as

$$\int_{S^-_{x_{\max}}}^{S^0_{x_{\max}}} S\rho(S)\,dS = \int_{S^0_{x_{\max}}}^{S^+_{x_{\max}}} S\rho(S)\,dS, \tag{6.2}$$

and

$$2(S^0_{x_{\max}})^2\rho(S^0_{x_{\max}}) < (S^-_{x_{\max}})^2\rho(S^-_{x_{\max}}) + (S^+_{x_{\max}})^2\rho(S^+_{x_{\max}}), \tag{6.3}$$

respectively, where S^*_x are defined in (6.17). Combining this with (4.7) and with the observation that $S^0_{x_{\max}} = S_{\max}$, $S^-_{x_{\max}} = S_1$, and $S^+_{x_{\max}} = S_2$, we get (4.8) and (4.9).

Third, if $\tau_0 < 0$, then one just recalls that $(x_{\max})_{\tau_0} = -(x_{\max})_{-\tau_0}$ by (4.16).

Now, let us state and prove the two auxiliary lemmas.

Lemma 6.1 *Let $\tau_0 = 0$ and let $\rho : [0,\infty) \to [0,\infty)$ be a bounded probability density function vanishing for $S > S_\rho$, where $0 < S_\rho \leqslant S_{\mathrm{tot}}$. Then $\mathcal{J}$ is differentiable on $\mathbb{R}\backslash\{0\}$, and*

$$\frac{d\mathcal{J}(x)}{dx} = -a\Big(\frac{u}{w}\Big)^2 \operatorname{sign} x \int_0^{S_x} S\rho(S)\,dS \qquad \forall x \neq 0, \tag{6.4}$$

where

$$S_x \equiv \Big(\frac{w}{ux}\Big)^2, \qquad w \equiv \frac{\delta}{S_0^{1/4}} > 0, \qquad u \equiv \frac{4h}{a\xi_0} > 0. \tag{6.5}$$

Remark 6.2 When $\tau_0 = 0$, the reason why $\mathcal{J}(x)$ is not differentiable at $x = 0$ is that $\Delta(-\frac{4h\sqrt{S}}{a\xi_0}x)$ attains the maximum at $x = 0$ for *every* S.

Proof [Proof of Lemma 6.1] For any $S' > 0$,

$$\left|\int_{S'-\epsilon}^{S'+\epsilon} \Delta(-u\sqrt{S}x)\sqrt{S}\rho(S)\,dS\right| \leqslant 2\frac{\epsilon}{w}\sup_{S>0}[\sqrt{S}\rho(S)] = O(\epsilon) \tag{6.6}$$

because ρ is bounded and vanishes for $S \geqslant S_\rho$. Hence,

$$\mathcal{J}(x) = au\lim_{\epsilon\to 0}\int_{(0,\infty)\backslash(S'-\epsilon,S'+\epsilon)} \Delta(-u\sqrt{S}x)\sqrt{S}\rho(S)\,dS, \tag{6.7}$$

implying

$$\begin{aligned}&\frac{\mathcal{J}(x+\varepsilon) - \mathcal{J}(x)}{\varepsilon}\\ &\quad = au\lim_{\epsilon\to 0}\int_{(0,\infty)\backslash(S'-\epsilon,S'+\epsilon)} \frac{\Delta(-u\sqrt{S}(x+\varepsilon)) - \Delta(-u\sqrt{S}x)}{\varepsilon}\sqrt{S}\rho(S)\,dS.\end{aligned} \tag{6.8}$$

If $\tau_0 = 0$ and $x \neq 0$, the function $\Delta(-u\sqrt{S}x)$ is smooth, except at $x = \pm\frac{w}{u\sqrt{S}}$. Thus, if $S \notin (S_x - \epsilon, S_x + \epsilon)$, the function $\Delta(-u\sqrt{S}x)$ is smooth on a small neighborhood of x, and we can write the expansion

$$\Delta(-u\sqrt{S}(x+\varepsilon)) - \Delta(-u\sqrt{S}x) = -u\sqrt{S}\varepsilon\frac{d\Delta(-u\sqrt{S}x)}{d\tau} + O(\varepsilon^2), \tag{6.9}$$

provided $|\varepsilon|$ is small enough. Consequently, the limit $\lim_{\varepsilon\to 0}\frac{\mathcal{J}(x+\varepsilon)-\mathcal{J}(x)}{\varepsilon}$ exists, it equals the derivative $\frac{d\mathcal{J}(x)}{dx}$, and, by virtue of (6.8),

$$\frac{d\mathcal{J}(x)}{dx} = -au^2\lim_{\epsilon\to 0}\int_{(0,\infty)\setminus(S_x-\epsilon,S_x+\epsilon)}\frac{d\Delta(-u\sqrt{S}x)}{d\tau}S\rho(S)\,dS. \tag{6.10}$$

This proves the differentiability of $\mathcal{J}(x)$ on $\mathbb{R}\setminus\{0\}$. Next, realizing that

$$-\frac{w}{u\sqrt{S}} < x < \frac{w}{u\sqrt{S}} \quad\Longleftrightarrow\quad -w < -u\sqrt{S}x < w \quad \forall 0 < S < S_x, \tag{6.11}$$

the value $-u\sqrt{S}x$ lies inside the support of the function $\Delta(\tau)$ for every $0 < S < S_x$. So, taking into account that

$$w^2\frac{d\Delta(-u\sqrt{S}x)}{d\tau} = \begin{cases}\operatorname{sign} x, & 0 < S < S_x,\\ 0, & S > S_x,\end{cases} \tag{6.12}$$

from (6.10) it follows that

$$\frac{d\mathcal{J}(x)}{dx} = -a\left(\frac{u}{w}\right)^2\operatorname{sign} x\lim_{\epsilon\to 0}\int_0^{S_x-\epsilon}S\rho(S)\,dS, \tag{6.13}$$

and we arrive at (6.4). □

Lemma 6.3 *Let $\tau_0 \neq 0$ and let $\rho : [0,\infty) \to [0,\infty)$ be a continuous probability density function vanishing for $S \geqslant S_\rho$, where $0 < S_\rho \leqslant S_{\text{tot}}$. Then $\mathcal{J}(x)$ is twice differentiable, and*

$$\left.\begin{aligned}\frac{d\mathcal{J}(x)}{dx} &= -a\left(\frac{u}{w}\right)^2\left(\int_{S_x^-}^{S_x^0} - \int_{S_x^0}^{S_x^+}\right)S\rho(S)\,dS\\ \frac{d^2\mathcal{J}(x)}{dx^2} &= 2\frac{a}{x}\left(\frac{u}{w}\right)^2[2(S_x^0)^2\rho(S_x^0) - (S_x^-)^2\rho(S_x^-) - (S_x^+)^2\rho(S_x^+)]\end{aligned}\right\}\ \forall x < 0, \tag{6.14}$$

$$\frac{d[\mathcal{J}(x)]_{\tau_0}}{dx} = -\frac{d[\mathcal{J}(-x)]_{-\tau_0}}{d(-x)}, \qquad \frac{d^2[\mathcal{J}(x)]_{\tau_0}}{dx^2} = \frac{d^2[\mathcal{J}(-x)]_{-\tau_0}}{d(-x)^2}, \tag{6.15}$$

and

$$\frac{d\mathcal{J}(0)}{dx} = \begin{cases}-a(\frac{u}{w})^2\operatorname{sign}\tau_0\int_0^\infty S\rho(S)\,dS, & |\tau_0| < w,\\ 0, & |\tau_0| \geqslant w,\end{cases} \qquad \frac{d^2\mathcal{J}(0)}{dx^2} = 0. \tag{6.16}$$

Here

$$S_x^0 \equiv \begin{cases}(\frac{\tau_0}{ux})^2, & \tau_0 > 0,\\ 0, & \tau_0 \leqslant 0,\end{cases} \qquad S_x^\pm \equiv \begin{cases}(\frac{\tau_0\pm w}{ux})^2, & \tau_0 > \mp w,\\ 0, & \tau_0 \leqslant \mp w,\end{cases} \tag{6.17}$$

and w, u were defined in (6.5).

Proof Using similar arguments to those leading to (6.8), we obtain

$$\frac{\mathcal{J}(x+\varepsilon)-\mathcal{J}(x)}{\varepsilon} = au\lim_{\epsilon\to 0}\int_{(0,\infty)\setminus U_\epsilon(x)} \frac{\Delta(-u\sqrt{S}(x+\varepsilon))-\Delta(-u\sqrt{S}x)}{\varepsilon}\sqrt{S}\rho(S)\,dS \tag{6.18}$$

with $U_\epsilon(x)\equiv\cup_{S\in\mathcal{M}(x)}(S-\epsilon,S+\epsilon)$, where the set

$$\mathcal{M}(x)\equiv\{0<S<\infty : -u\sqrt{S}x=\tau_0\vee -u\sqrt{S}x=\tau_0\pm w\} \tag{6.19}$$

contains at most three elements. The function $\Delta(-u\sqrt{S}x)$ is smooth, except at $x=-\frac{\tau_0}{u\sqrt{S}}$ and $x=-\frac{\tau_0\pm w}{u\sqrt{S}}$. Thus, if $S\notin U_\epsilon(x)$, the function $\Delta(-u\sqrt{S}x)$ is smooth on a small neighborhood of x, and we can write the expansion (6.9), provided $|\varepsilon|$ is small enough. Plugging the expansion into (6.18), we observe that the limit $\lim_{\varepsilon\to 0}\frac{\mathcal{J}(x+\varepsilon)-\mathcal{J}(x)}{\varepsilon}$ exists, it equals the derivative $\frac{d\mathcal{J}(x)}{dx}$, and

$$\frac{d\mathcal{J}(x)}{dx} = -au^2\lim_{\epsilon\to 0}\int_{(0,\infty)\setminus U_\epsilon(x)}\frac{d\Delta(-u\sqrt{S}x)}{d\tau}S\rho(S)\,dS. \tag{6.20}$$

This proves the differentiability of $\mathcal{J}(x)$ on $\mathbb{R}$.

From (4.2) we have

$$w^2\frac{d\Delta(\tau)}{d\tau}=\begin{cases}1, & \tau_0-w<\tau<\tau_0,\\ -1, & \tau_0<\tau<\tau_0+w,\\ 0, & \tau\in\mathbb{R}\setminus[\tau_0-w,\tau_0+w].\end{cases} \tag{6.21}$$

Combined with

$$\begin{aligned}
\tau_0-w<-u\sqrt{S}x<\tau_0 &\iff S_x^-<S<S_x^0,\\
\tau_0<-u\sqrt{S}x<\tau_0+w &\iff S_x^0<S<S_x^+,\\
-u\sqrt{S}x<\tau_0-w &\iff 0<S<S_x^-,\\
-u\sqrt{S}x>\tau_0+w &\iff S>S_x^+,
\end{aligned}\qquad \forall x<0 \tag{6.22}$$

and with

$$\mathcal{M}(x)=\begin{cases}\{S_x^-,S_x^0,S_x^+\}, & \tau_0>w,\\ \{S_x^0,S_x^+\}, & 0<\tau_0\leqslant w,\\ \{S_x^+\}, & -w<\tau_0\leqslant 0,\\ \emptyset, & \tau_0\leqslant -w,\end{cases}\qquad \forall x<0 \tag{6.23}$$

(6.17) and (6.20) imply the first equality in (6.14). Using (6.17) again together with the identity

$$\frac{d}{dx}\int_0^{S_x^*}S\rho(S)\,dS=-\frac{2}{x}(S_x^*)^2\rho(S_x^*) \tag{6.24}$$

following from the Second fundamental theorem of the Integral calculus, from the first equality in (6.14) we readily obtain the second one.

The equalities in (6.15) immediately follow from Statement 4.1(1).

Finally, (6.16) is obtained from (6.14) by taking the limit $x \to 0^-$ and, in the second equality, also by realizing that $\rho(0) = 0$ and that $\rho(S) = 0$ for all $S \geqslant S_\rho$. □

6.3 Part (3)

By virtue of (4.5) and (4.7),

$$H = \frac{4h}{\xi_0} \int_0^\infty \sqrt{S} \Delta\left(\tau_0 \sqrt{\frac{S}{S_{\max}}}\right) \rho(S)\, dS. \tag{6.25}$$

Observing that

$$\Delta\left(\tau_0 \sqrt{\tfrac{S}{S_{\max}}}\right) = \begin{cases} \frac{S_0^{1/4}}{\delta}(1 - |x_S|), & S_1 < S < S_2, \\ 0, & S \in (0, \infty) \setminus (S_1, S_2), \end{cases} \tag{6.26}$$

we immediately arrive at (4.11).

6.4 Part (4)

Using (4.5) and the substitution $\tau = -\frac{4h\sqrt{S}}{a\xi_0} x$, we have

$$A = \frac{4h}{\xi_0} \int_0^\infty \left[\int_{\mathbb{R}} \Delta\left(-\frac{4h\sqrt{S}}{a\xi_0} x\right) dx \right] \sqrt{S} \rho(S)\, dS = a \int_{\mathbb{R}} \Delta(\tau)\, d\tau = a. \tag{6.27}$$

Similarly,

$$\begin{aligned} \alpha &= \frac{4h}{a\xi_0} \int_0^\infty \left[\int_{-\infty}^{\psi_{\max}} \Delta\left(-\frac{4h\sqrt{S}}{a\xi_0} x\right) dx \right] \sqrt{S} \rho(S)\, dS \\ &= \int_0^\infty \left(\int_{\tau_0 \sqrt{\frac{S}{S_{\max}}}}^\infty \Delta(\tau) d\tau \right) \rho(S)\, dS. \end{aligned} \tag{6.28}$$

Observing that

$$\int_{\tau_0 \sqrt{\frac{S}{S_{\max}}}}^\infty \Delta(\tau)\, d\tau = \begin{cases} 0 & \tau_0 \sqrt{\frac{S}{S_{\max}}} \geqslant \tau_0 + w, \\ \frac{1 - x_S(2 - |x_S|)}{2} & \tau_0 - w \leqslant \tau_0 \sqrt{\frac{S}{S_{\max}}} \leqslant \tau_0 + w, \\ 1 & \tau_0 \sqrt{\frac{S}{S_{\max}}} \leqslant \tau_0 - w, \end{cases} \tag{6.29}$$

and that

$$\begin{aligned}
\tau_0\sqrt{\frac{S}{S_{\max}}} \geqslant \tau_0 + w \quad &\Longleftrightarrow \quad \begin{cases} S \geqslant S_2, & \tau_0 > 0, \\ S \leqslant S_1, & \tau_0 < 0, \end{cases} \\
\tau_0 - w \leqslant \tau_0\sqrt{\frac{S}{S_{\max}}} \leqslant \tau_0 + w \quad &\Longleftrightarrow \quad S_1 \leqslant S \leqslant S_2, \\
\tau_0\sqrt{\frac{S}{S_{\max}}} \leqslant \tau_0 - w \quad &\Longleftrightarrow \quad \begin{cases} S \leqslant S_1, & \tau_0 > 0, \\ S \geqslant S_2, & \tau_0 < 0, \end{cases}
\end{aligned} \tag{6.30}$$

we obtain (4.14).

6.5 Verification of (4.18)

The limit $\tau_0 \to \pm\infty$ is equivalent to the limit $c \to \pm\infty$ by (4.10). Thus, taking into account that $S_1 = (1 - \frac{1}{|c|})^2 S_{\max}$ for $|c| \geqslant 1$ and that $S_2 = (1 + \frac{1}{|c|})^2 S_{\max}$, we observe that $0 \leqslant \frac{1 - x_S(2 - |x_S|)}{2} \leqslant 1$ for $S_1 \leqslant S \leqslant S_2$ and $|c| \geqslant 1$, implying

$$\begin{aligned}
0 &\leqslant \lim_{\tau_0 \to \pm\infty} \int_{S_1}^{S_2} \frac{1 - x_S(2 - |x_S|)}{2} \rho(S)\, dS \\
&\leqslant \sup_{0 < S < S_\rho} \rho(S) \lim_{c \to \pm\infty} \left[\left(1 + \frac{1}{|c|}\right)^2 - \left(1 - \frac{1}{|c|}\right)^2 \right] S_\rho = 0.
\end{aligned} \tag{6.31}$$

Therefore,

$$\lim_{\tau_0 \to \pm\infty} \alpha = \lim_{c \to \pm\infty} \alpha_0 = \lim_{c \to \pm\infty} \begin{cases} \int_0^{(1-\frac{1}{|c|})^2 S_{\max}} \rho(S)\, dS, & \text{if } \tau_0 \geqslant 0, \\ \int_{(1+\frac{1}{|c|})^2 S_{\max}}^{\infty} \rho(S)\, dS, & \text{if } \tau_0 \leqslant 0 \end{cases} \tag{6.32}$$

by (4.14). Combining this with the fact that $\lim_{c \to \infty} S_{\max}(c) = \lim_{c \to -\infty} S_{\max}(c)$ due to (4.6), we get (4.18).

Let $|c|$ be now sufficiently large. Then, in order to find $S_{\max}^{\infty}$, the relations (4.8) and (4.9) read

$$\begin{aligned}
0 &= \left(\int_{(1-\frac{1}{|c|})^2 S_{\max}}^{S_{\max}} - \int_{S_{\max}}^{(1+\frac{1}{|c|})^2 S_{\max}} \right) S\rho(S)\, dS \\
&= -2S_{\max}^2 \left[3\rho(S) + 2S \frac{d\rho(S)}{dS} \right]_{S_{\max}} \frac{1}{c^2} + O\left(\frac{1}{c^4}\right) \\
&= -4S_{\max}^{3/2} \frac{d\tilde{\rho}(S_{\max})}{dS} \frac{1}{c^2} + O\left(\frac{1}{c^4}\right)
\end{aligned} \tag{6.33}$$

and

$$0 < 2S_{\max}^2\rho(S_{\max}) - \left[\left(1-\frac{1}{|c|}\right)^2 S_{\max}\right]^2 \rho\left(\left(1-\frac{1}{|c|}\right)^2 S_{\max}\right) - \left[\left(1+\frac{1}{|c|}\right)^2 S_{\max}\right]^2 \rho\left(\left(1+\frac{1}{|c|}\right)^2 S_{\max}\right) = -2S_{\max}^{3/2}\left[3\frac{d\tilde{\rho}(S_{\max})}{dS} + 2S_{\max}\frac{d^2\tilde{\rho}(S_{\max})}{dS^2}\right]\frac{1}{c^2} + O\left(\frac{1}{c^4}\right), \tag{6.34}$$

respectively, where $\tilde{\rho}(S) \equiv S^{3/2}\rho(S)$. Thus, if $\frac{d\tilde{\rho}(S_{\max})}{dS} = 0$ and $\frac{d^2\tilde{\rho}(S_{\max})}{dS^2} < 0$, the relations (4.8) and (4.9) are satisfied up to the order $O(\frac{1}{c^4})$.

Acknowledgements This research was supported by the Robert A. Welch Foundation, grant P-0446, and by the grants VEGA 1/3031/06 and CGA V/4/2005. I.M. would like to thank D.A.H. and express his appreciation for the hospitality extended to him during his stays at TCU.

Appendix Shape average revisited

In our analysis we have neglected the fact that the dimensionless parameter $\xi_C \equiv \frac{B_C}{\sqrt{S_C}}$ defined in (2.14) that characterizes the crystal shape may change from crystal to crystal, and we considered it constant for all the crystals (see (As6)). In this appendix we discuss the modifications to our theory in the case when ξ_C is not fixed.

In order to carry out the argument easily and explicitly, we will conveniently use the Gaussian function

$$\mathcal{G}(y; w, \mathcal{A}) \equiv \frac{\mathcal{A}}{w} e^{-\pi(\frac{y}{w})^2} \tag{7.1}$$

that attains its maximum at $y = 0$ and has the area $\mathcal{A}$, the height $\frac{\mathcal{A}}{w}$, and the half-width $\sqrt{\frac{\log 8}{\pi}}w \doteq 0.94w$. The reason we work with the Gaussian $\mathcal{G}$ is that we can easily perform the integrations of the form

$$\int_{-\infty}^{\infty} \mathcal{G}(y - y_1; w_1, \mathcal{A}_1)\mathcal{G}(y - y_2; w_2, \mathcal{A}_2)\, dy = \mathcal{G}(y_1 - y_2; \sqrt{w_1^2 + w_2^2}, \mathcal{A}_1\mathcal{A}_2) \tag{7.2}$$

and use the scaling property

$$\mathcal{G}(by; w, \mathcal{A}) = \frac{1}{b}\mathcal{G}\left(y; \frac{w}{b}, \mathcal{A}\right), \quad b \neq 0. \tag{7.3}$$

If ξ_C varies from crystal to crystal, the current density $J_E^{\omega_E}(\psi)$ is a triple average given by (3.18) rather than the double average given by (3.23). Thus, we first need to evaluate the discrete shape average that we will approximate by the integral

$$\langle j_C(S, \tau, \xi, \psi)\rangle_\xi \approx \int j_C(S, \tau, \xi, \psi) p_{S,\tau}(\xi)\, d\xi, \tag{7.4}$$

where $p_{S,\tau}(\xi)$, the continuous version of the fraction $\mathbb{P}_\xi^{(S,\tau)}$, is for simplicity assumed Gaussian, i.e.,

$$p_{S,\tau}(\xi) = \mathcal{G}(\xi - \xi_0; w_\xi, 1). \tag{7.5}$$

Here ξ_0 is the mean value of ξ and w_ξ is sufficiently small so that the crystal shape is not too oblong (i.e., $\xi_0 + w_\xi \leqslant \hat{\xi}$ and $\xi_0 - w_\xi \geqslant \check{\xi}$, see (As3) and Remark 2.7(iii)). Unlike in the case of the function $p_S(\tau)$ from (As7) (see Subsection 4.2.1), the dependence of ξ_0 and w_ξ on the crystal size S (and also on τ) is hard to perceive. Therefore, for the sake of argument, let us simply suppose that both ξ_0 and w_ξ are independent of S and τ.

Approximating the $\cosh^{-2}$ spike in (3.22) by a Gaussian spike $\mathcal{G}$ with the same maximum position, area, and height, the current density from a single crystal can be expressed as

$$j_C(S,\tau,\xi,\psi) \approx \mathcal{G}(\psi - \psi_C(S,\tau,\xi); w_0, a) \quad \text{with } w_0 \equiv \frac{a}{h\beta S}. \tag{7.6}$$

Combined with (7.2) through (7.5) and (3.20), we get

$$\langle j_C(S,\tau,\xi,\psi)\rangle_\xi \approx \mathcal{G}(\psi - \psi_C(S,\tau,\xi_0); w_1, a) \quad \text{with} \quad w_1 \equiv \sqrt{w_0^2 + \Big(\frac{a\tau}{4h\sqrt{S}} w_\xi\Big)^2}. \tag{7.7}$$

Notice that in the limit $w_\xi \to 0$ (uniform shape of all the crystals) we have $w_1 \to w_0$ and, correctly, (7.7) reduces to (7.6).

Assuming that $p_S(\tau)$ is also Gaussian, $p_S(\tau) = \mathcal{G}(\tau - \tau_0; w_\tau, 1)$ (c.f. (As7)), we can similarly evaluate the average over the boundary tension. We find

$$\langle\langle j_C(S,\tau,\xi,\psi)\rangle_\xi\rangle_\tau \approx \mathcal{G}(\psi - \psi_C(S,\tau_0,\xi_0); w_2, a), \tag{7.8}$$

where

$$w_2 \equiv \sqrt{w_0^2 + \Big(\frac{a\tau_0}{4h\sqrt{S}} w_\xi\Big)^2 + \Big(\frac{a\xi_0}{4h\sqrt{S}} w_\tau\Big)^2} \approx \frac{a\xi_0}{4h\sqrt{S}} \sqrt{w_\tau^2 + \Big(\frac{\tau_0}{\xi_0} w_\xi\Big)^2}. \tag{7.9}$$

In the last step we neglected the term $w_0^2 \propto S^{-2}$ in the square root, for it is small with respect to the third term ($w_\tau \propto S^{-1/4}$ by (As7)).

We may now compare (7.8) with the dominant term $\mathcal{D}_S(\psi)$ from Statement 3.14, i.e., with a result in which the ξ-average was not taken into account. Clearly, the main difference concerns only the change of the height (or, equivalently, the half-width) of the resulting spike. Namely, in the present situation the height is $\frac{a}{w_2}$, while the height of $\mathcal{D}_S(\psi)$ corresponds to $\frac{a}{(w_2)_{w_\xi=0}}$. Thus, the effect of the ξ-averaging may be symbolically written as the substitution

$$w_\tau \longrightarrow \sqrt{w_\tau^2 + \Big(\frac{\tau_0}{\xi_0} w_\xi\Big)^2}. \tag{7.10}$$

Thus, whenever

$$w_\tau \gg \frac{\tau_0}{\xi_0} w_\xi, \tag{7.11}$$

the average over the values of ξ has practically no effect, and it may be well neglected, as was done in (As6). As a matter of fact, the condition (7.11) can be simply checked, using the experimental characteristics of the voltammogram. In particular, it is true for the three experimental voltammograms to which we will applied our theory in Sect. 4 (see Table 1).

References

1. Kolb, D.M.: Physical and electrochemical properties of metal monolayers on metallic substrates. In: Advances in Electrochemistry and Electrochemical Engineering, vol. 11, pp. 125–271. Wiley, New York (1978)
2. Huckaby, D.A., Blum, L.: A model for sequential first-order phase transitions occurring in the underpotential deposition of metals. J. Electroanal. Chem. **315**, 255–261 (1991)
3. Blum, L., Huckaby, D.A.: Underpotential deposition of Cu on Au(111): implications of the HB model. J. Electroanal. Chem. **375**, 69–77 (1994)
4. Huckaby, D.A., Blum, L.: Rigorous analysis of low-temperature phases in a model for underpotential deposition of copper on the (111) surface of gold in the presence of bisulfate. Langmuir **11**, 4583–4587 (1995)
5. Huckaby, D.A., Legault, M.D., Blum, L.: Cluster variation study of the underpotential deposition of Cu on Au(111) in the presence of bisulfate. J. Chem. Phys. **109**, 3600–3606 (1998)
6. Blum, L., Huckaby, D.A.: Phase transitions at liquid-solid interfaces: Padé approximant to adsorption isotherms and voltammograms. J. Chem. Phys. **94**, 6887–6894 (1991)
7. Brown, G., Rikvold, P.A., Mitchell, S.J., Novotny, M.A.: Monte Carlo methods for equilibrium and nonequilibrium problems in interfacial electrochemistry. In: Interfacial Electrochemistry: Theory, Experiment, and Applications, pp. 47–61. Dekker, New York (1999)
8. Rikvold, P.A., Brown, G., Mitchell, S.J.: Statistical mechanics of lattice models of electrochemical interfaces. In: Encyclopedia of Surface and Colloid Science, pp. 4814–4824. Dekker, New York (2002)
9. Zhang, J., Sung, Y.-E., Rikvold, P.A., Wieckowski, A.: Underpotential deposition of Cu on Au(111) in sulfate-containing electrolytes: a theoretical and experimental study. J. Chem. Phys. **104**, 5699–5712 (1996)
10. Brown, G., Rikvold, P.A., Novotny, M.A., Wieckowski, A.: Simulated dynamics of underpotential deposition of Cu with sulfate on Au(111). J. Electrochem. Soc. **146**, 1035–1040 (1999)
11. Huckaby, D.A., Medved', I.: Shapes of voltammogram spikes explained as resulting from the effects of finite electrode crystal sizes. J. Chem. Phys. **117**, 2914–2922 (2002)
12. Medved', I., Huckaby, D.A.: Voltammogram spikes interpreted as envelopes of spikes resulting from electrode crystals of various sizes: application to the UPD of Cu on Au(111). J. Chem. Phys. **118**, 11147–11159 (2003)
13. Borgs, C., Kotecký, R.: Surface-induced finite-size effects for the first-order phase transitions. J. Stat. Phys. **79**, 43–116 (1995)
14. Zahradník, M.: An alternate version of Pirogov–Sinai theory. Commun. Math. Phys. **93**, 559–581 (1984)
15. Borgs, C., Imbrie, J.Z.: A unified approach to phase diagrams in field theory and statistical mechanics. Commun. Math. Phys. **123**, 305–328 (1989)
16. van Enter, A.C.D., Ferndández, R., Sokal, A.D.: Regularity properties and pathologies of position-space renormalization-group transformations: scope and limitations of Gibbsian theory. J. Stat. Phys. **72**, 879–1167 (1993)
17. Kotecký, R., Preiss, D.: Cluster expansions for abstract polymer models. Commun. Math. Phys. **103**, 491–498 (1986)
18. Bovier, A., Zahradník, M.: A simple inductive approach to the problem of convergence of cluster expansions of polymer models. J. Stat. Phys. **100**, 765–778 (2000)
19. Miracle-Solé, S.: On the convergence of cluster expansions. Physica A **279**, 244–249 (2000)
20. Sokal, A.D.: Chromatic polynomials, Potts models, and all that. Physica A **279**, 324–332 (2000)
21. Zahradník, M.: A short course on the Pirogov–Sinai theory. Rend. Mat. Ser. VII **18**, 411–486 (1998)
22. Kotecký, R.: Phase transitions: on a crossroads of probability and analysis. In: Highlights of Mathematical Physics, pp. 191–207. Amer. Math. Soc., Providence (2002)
23. Borgs, C., Kotecký, R.: A rigorous theory of finite-size scaling at first-order phase transitions. J. Stat. Phys. **61**, 79–119 (1990)
24. van Enter, A.C.D., Medved', I., Netočný, K.: Chaotic size dependence in the Ising model with random boundary conditions. Markov Proc. Rel. Fields **8**, 479–508 (2002)
25. Ruelle, D.: Statistical Mechanics: Rigorous Results. Benjamin, Reading (1969)
26. White, J.H., Abruña, H.D.: Coadsorption of copper with anions on platinum (111): the role of surface redox chemistry in determining the stability of a metal monolayer. J. Chem. Phys. **94**, 894–900 (1990)
27. Bittner, A.M., Wintterlin, J., Ertl, G.: Strain relief during metal-on-metal electrodeposition: a scanning tunneling microscopy study of copper growth on Pt(100). Surf. Sci. **376**, 267–278 (1997)
28. Kolb, D.M.: The initial stages of metal deposition: an atomistic view. In: Schering Lectures, vol. 2, pp. 5–35. Schering Research Foundation, Berlin (1991)
29. Yee, H.S., Abruña, H.D.: In-situ X-ray studies of the underpotential deposition of copper on platinum(111). J. Chem. Phys. **97**, 6278–6288 (1993)